Polypyrimidine Tract Binding Proteins are essential for B cell development

Authors:

Elisa Monzón-Casanova[1,2*], Louise S. Matheson[1], Kristina Tabbada[3], Kathi Zarnack[4], Christopher W. J. Smith[2] and Martin Turner[1*]

Affiliations:

[1]Laboratory of Lymphocyte Signalling and Development, The Babraham Institute, Cambridge, UK;

[2]Department of Biochemistry, University of Cambridge, Cambridge, UK;

[3]Next Generation Sequencing Facility, The Babraham Institute, Cambridge, UK;

[4]Buchmann Institute for Molecular Life Sciences, Goethe University Frankfurt, Frankfurt am Main, Germany

*Corresponding authors:

Elisa Monzón-Casanova (elisa.monzon-casanova@babraham.ac.uk) and Martin Turner (martin.turner@babraham.ac.uk)

Abstract

During B cell development, recombination of immunoglobulin loci is tightly coordinated with the cell cycle to avoid unwanted rearrangements of other genomic locations. Several factors have been identified that suppress proliferation in late-pre-B cells to allow light chain recombination. By comparison, our knowledge of factors limiting proliferation during heavy chain recombination at the pro-B cell stage is very limited. Here we identify an essential role for the RNA-binding protein Polypyrimidine Tract Binding Protein 1 (PTBP1) in B cell development. Absence of PTBP1 and the paralog PTBP2 results in a complete block in development at the pro-B cell stage. PTBP1 promotes the fidelity of the transcriptome in pro-B cells. In particular, PTBP1 controls a cell cycle mRNA regulon, suppresses entry into S-phase and promotes progression into mitosis. Our results highlight the importance of S-phase entry suppression and post-transcriptional gene expression control by PTBP1 in pro-B cells for proper B cell development.

Introduction

During development B cells first rearrange VDJ gene segments of their immunoglobulin heavy chain (Igh) locus and subsequently VJ gene segments from their immunoglobulin light (Igl) loci to generate antibody diversity (**Supplementary Fig. 1a**). A burst in proliferation at the early-pre-B cell stage occurs once developing B cells have successfully recombined their Igh locus (Herzog et al., 2009). V(D)J recombination occurs during G0/G1 phase of the cell cycle (Schlissel et al., 1993) and RAG proteins are degraded upon entry into S-phase to suppress V(D)J recombination (Li et al., 1996). Therefore, alternation between proliferative and non-proliferative stages during B cell development is precisely controlled (Herzog et al., 2009; Clark et al., 2014). Several factors have been identified that suppress proliferation in late-pre-B cells and allow Igl recombination including interferon regulatory factors-4 and -8 (Irf4, Irf8) (Lu et al., 2003), Ras (Mandal et al., 2009), Ikaros and Aiolos (Ma et al., 2010), BCL-6 (Nahar et al., 2011), dual specificity tyrosine-regulated kinase 1A (DYRK1A) (Thompson et al., 2015), B cell translocation gene 2 (BTG2) and protein arginine methyl transferase 1 (PRMT1) (Dolezal et al., 2017). By comparison, we are only beginning to understand mechanisms that control proliferation in pro-B cells. At this stage, cell cycle progression driven by IL-7 is segregated from Igh recombination (Johnson et al., 2012) and the RNA-binding proteins (RBPs) ZFP36L1 and ZFP36L2 suppress proliferation allowing Igh recombination and B cell development (Galloway et al., 2016).

A network of transcription factors controls development and identity in B cells (Busslinger, 2004). After transcription, RBPs control messenger RNA (mRNA) expression and coordinate functionally related genes in mRNA regulons (Keene, 2007). Control of

cell cycle mRNA regulons by RBPs is fundamental for early lymphocyte development (Galloway and Turner, 2017). Polypyrimidine Tract Binding Proteins (PTBP) are RBPs that control alternative splicing, alternative polyadenylation, mRNA stability and translation (Hu et al., 2018; Knoch et al., 2004; 2014). PTBP1 can either increase or decrease mRNA stability by binding to the 3'UTR of transcripts or by modulating alternative splicing of exons that will form transcript isoforms degraded by nonsense-mediated mRNA decay (NMD) (Hu et al., 2018). PTBP1 is expressed ubiquitously. PTBP2 and PTBP3 (formerly ROD1) are highly conserved paralogs of PTBP1 expressed in neurons and hematopoietic cells, respectively. PTBP1 suppresses expression of PTBP2 directly by inducing *Ptbp2* exon 10 skipping and mRNA degradation by NMD (Boutz et al., 2007). In germinal centre B cells, PTBP1 promotes proliferation, the c-MYC gene expression program induced upon positive selection and antibody affinity maturation (Monzon-Casanova et al., 2018). PTBP1 and PTBP2 have specific and redundant functions (Spellman et al., 2007; Vuong et al., 2016; Ling et al., 2016). Therefore, expression of PTBP2 in PTBP1-deficient cells compensates for many functions of PTBP1 (Spellman et al., 2007; Vuong et al., 2016; Ling et al., 2016; Monzon-Casanova et al., 2018).

To study the roles of PTBP1 controlling post-transcriptional gene expression in B cells, we and others deleted *Ptbp1* in pro-B cells and found normal B cell development accompanied by PTBP2 expression (Monzon-Casanova et al., 2018; Sasanuma et al., 2019). Here we addressed the functions of PTBP in B cell development by deleting both *Ptbp1* and *Ptbp2* in pro-B cells. We show that PTBP1, and in its absence PTBP2, are essential to promote B cell lymphopoiesis. In pro-B cells PTBP1 suppresses entry into S-phase and promotes entry into mitosis after G2-phase. At the molecular level, PTBP1 is

necessary to maintain transcriptome fidelity in pro-B cells and is an essential component of a previously unrecognised cell cycle mRNA regulon.

Results

Redundancy between PTBP1 and PTBP2 for B cell development

As both PTBP1 and PTBP3 are expressed in mature B cells (Monzon-Casanova et al., 2018) we determined their expression during defined stages of B cell development in mouse bone marrow (**Supplementary Fig. 1a-d**). Fluorescence intensity of intracellular PTBP1 staining by flow cytometry was greater in pro- and early-pre-B cells compared to late-pre-B and immature-B cells. However, the isotype control staining for PTBP1 showed the same differences in fluorescence intensity (**Supplementary Fig. 1c, d**). Therefore, PTBP1 protein expression was similar between the different bone marrow B cell populations. PTBP3 protein detected with a specific monoclonal antibody (Monzon-Casanova et al., 2018) was also relatively constant throughout B cell development (**Supplementary Fig. 1c, d**). PTBP2 protein was not detected in any of the B cell developmental stages analysed (**Supplementary Fig. 1c, d**). Thus, PTBP1 and PTBP3, but not PTBP2, are co-expressed throughout B cell development.

Conditional deletion of a *Ptbp1*-floxed allele (Suckale et al., 2011) in pro-B cells with the *Cd79a*^{cre} allele (*Cd79a*$^{cre/+}$*Ptbp1*$^{fl/fl}$ mice, denoted here as *Ptbp1* single conditional knock-out, P1sKO) did not affect B cell development and resulted in the expression of PTBP2 (Monzon-Casanova et al., 2018). Therefore, we generated a double conditional knock-out (dKO) mouse model where both *Ptbp1* and *Ptbp2* were deleted in pro-B cells using floxed alleles and *Cd79a*^{cre} (*Cd79a*$^{cre/+}$*Ptbp1*$^{fl/fl}$*Ptbp2*$^{fl/fl}$ mice, denoted here as P1P2dKO). Deletion of both *Ptbp1* and *Ptbp2* in pro-B cells resulted in the absence of mature B cells in the spleen and lymph nodes (**Fig. 1a, b** and **Supplementary Fig. 1e**).

PTBPs are required for progression beyond the pro-B cell stage

The absence of mature B cells in P1P2dKO mice resulted from a block in B cell development at the pro-B cell stage (**Fig. 1c, d** and **Supplementary Fig. 1a**). We confirmed the lack of PTBP proteins in pro-B cells from the conditional KO mice (**Supplementary Fig. 2a, b**). PTBP1 protein was absent in P1sKO and P1P2dKO pro-B cells and *Ptbp1* deletion led to the expression of PTBP2 in P1sKO pro-B cells (**Supplementary Fig. 2b**). P1P2dKO pro-B cells failed to increase PTBP2 in response to *Ptbp1* deletion, validating our dKO. P1P2dKO pro-B cells expressed increased amounts of PTBP3 compared to pro-B cells from littermate control mice (*Cd79a*$^{+/+}$*Ptbp1*$^{fl/fl}$*Ptbp2*$^{fl/fl}$, denoted here as "control" unless stated otherwise) (**Supplementary Fig. 2b**). Yet, PTBP3 was insufficient to compensate for the lack of PTBP1 and PTBP2 in pro-B cells (**Fig. 1c, d**), demonstrating an irreplaceable role for PTBP1 in B cell development in the absence of PTBP2.

Characterisation of B cell development distinguishing between pro-, early- and late-pre-B cells revealed an increase in the numbers of early-pre-B cells in P1sKO compared to control mice and to *Cd79a*^{cre} "Cre-only" mice (mb1, *Cd79a*$^{Cre/+}$*Ptbp1*$^{+/+}$*Ptbp2*$^{+/+}$) (**Fig. 1d**). In contrast, the numbers of late-pre- and immature-B cells were similar between P1sKO and control mice (**Fig. 1d**). These data confirmed that deletion of *Ptbp1* alone results in largely unaffected B cell development.

In P1P2dKO mice there were similar numbers of FrB pro-B cells (B220^{+}, CD19^{+}, IgM^{-}, CD43^{high}, CD24^{+}, CD249^{low}) and FrC pro-B cells (B220^{+}, CD19^{+}, IgM^{-}, CD43^{high}, CD24^{+}, CD249^{high}) compared to littermate control and to *Cd79a*^{cre} "Cre-only" mice but we did not find FrC' early-pre-B cells, characterised by high expression of CD24 and CD249 (detected

by BP-1) (**Fig. 1d**). P1P2dKO FrB and FrC pro-B cells have higher CD24 staining than control FrB and FrC pro-B cells (**Fig. 1c**). Therefore, we set different gates in the P1P2dKO mice to include all these cells. FrB and FrC pro-B cells from P1P2dKO mice showed increased c-KIT (CD117) staining compared to P1sKO and control pro-B cells and lacked CD2, corroborating a block at an early developmental stage (**Supplementary Fig. 2c**, **d**). With a cell surface and intracellular staining (**Supplementary Fig. 2a**) to identify early and late pre-B cells as cells with successfully rearranged intracellular Igμ chain we confirmed the block in B cell development in P1P2dKO mice at the pro-B cell stage (**Supplementary Fig. 2a, e**). With this gating strategy the numbers of pro-B cells in P1P2dKO mice were reduced compared to P1sKO and control mice. Few early-pre-B cells ($B220^+$, $CD19^+$, IgM^-, $CD93^+$, $CD43^{high}$, $Ig\mu^+$) were present in P1P2dKO mice indicating some successful recombination of the Igh locus in P1P2dKO pro-B cells (**Supplementary Fig. 2a**). However, the numbers of early-pre-B cells were decreased by ~13-fold in P1P2dKO compared to control mice (**Supplementary Fig. 2e**). Compared to the numbers of pro-B cells in *Rag2*$^{-/-}$ deficient mice, the numbers of P1P2dKO pro-B cells identified by the two different staining strategies were decreased by ~4.6-fold (FrB), 19-fold (FrC) (**Fig. 1d**) and 47-fold (pro-B, **Supplementary Fig. 2e**). Thus, when Igh recombination is defective in *Rag2*$^{-/-}$ mice developing B cells accumulate at the pro-B cell stage, whereas in P1P2dKO mice pro-B cells do not accumulate.

PTBP1 suppresses entry into S-phase in pro-B cells

Dynamic control of proliferation is essential for successful B cell development (Clark et al., 2014; Galloway and Turner, 2017). Therefore, we assessed the proliferative status of pro-B cells in the P1P2dKO mice. To identify cells in early-, late- or post-S-phase we sequentially labelled cells *in vivo* with EdU and BrdU (**Fig. 2a**). With this approach, cells

that incorporate only EdU were in S-phase at the beginning, but not at the end of the labelling period and are in post S-phase; cells that incorporate both EdU and BrdU are in late S-phase; and cells labelled only with BrdU at the end of the labelling period are in early S-phase. In control mice, we detected few pre-pro-B cells in S-phase (3.8% in early- and late-S together), compared to 13% of pro-B cells and high frequencies (53%) of early-pre-B cells in S-phase (**Supplementary Fig. 3a-d**). In P1P2dKO pro-B cells the proportions of early-S-phase cells were increased 4.7-fold compared to control and 3.2-fold compared to P1sKO pro-B cells (**Fig. 2b, c**). The numbers of early-S-phase P1P2dKO pro-B cells were similar to those of P1sKO and control pro-B cells (**Fig. 2d**). However, the numbers of the whole pro-B cell population identified with the combination of cell surface and intracellular markers ($IgD^{-}IgM^{-}B220^{+}CD19^{+}CD43^{high}Ig\mu^{+}$) used with the EdU and BrdU labelling approach (**Supplementary Fig. 3a**) were reduced 4.4-fold in P1P2dKO compared to control mice (**Fig. 2d**). Therefore, it is unlikely that the increased proportions in early S-phase amongst P1P2dKO pro-B cells result from reduced numbers of pro-B cells in G0/G1-phase. Thus, in the absence of PTBP1 and PTBP2 pro-B cells enter S-phase more readily. The proportions of P1P2dKO pro-B cells in late S-phase and post S-phase were also increased compared to P1sKO pro-B cells and control pro-B cells (**Fig. 2c**). The magnitude of the increase in the proportions of cells in post S-phase was smaller than the increase in either early- or late-S-phase. This indicated that P1P2dKO pro-B cells enter S-phase more readily than control pro-B cells but they fail to progress through S-phase at the same pace as PTBP1-sufficient pro-B cells.

PTBP1 is required for the transition from G2 to M phase in pro-B cells

We also analysed cells in G2/M-phases by detecting DNA synthesis in combination with DNA content (**Fig. 2e**, **Supplementary Fig. 3e, f**). The proportion of P1P2dKO pro-B cells

in G2/M-phase was increased ~40-fold compared to P1sKO and control pro-B cells (**Fig. 2e, f**) and the numbers of G2/M-phase pro-B cells in P1P2dKO mice were increased ~8-fold compared to control and P1sKO mice (**Fig. 2e, f**). These findings were confirmed when identifying FrB pro-B cells using cell surface markers ($CD19^+$, $CD24^+$, $CD249^-$, $CD2^-$, $CD25^-$, IgM^-, IgD^-), EdU labelling and DNA staining (**Supplementary Fig. 3g, h**). To preserve phosphorylated histone 3 (pH3), which marks cells in mitosis, during the staining process and quantitating DNA content with sufficient resolution, we identified FrB pro-B cells again with cell surface markers ($CD19^+$, $CD24^+$, $CD249^-$, $CD2^-$, $CD25^-$, IgM^-, IgD^-) (**Supplementary Fig. 3g, i**). Some P1P2dKO pro-B cells had high pH3 levels amongst cells with 4N-DNA content (**Supplementary Fig. 3i**). However, the proportions of pH3-positive cells amongst P1P2dKO pro-B cells with 4N-DNA content were reduced compared to the proportions found amongst P1sKO and control pro-B cells (**Supplementary Fig. 3i, j**). Therefore, the majority of P1P2dKO pro-B cells with 4N-DNA content are in G2-phase and have not entered mitosis. PTBP1 is thus required in pro-B cells to progress from G2 to M-phase of the cell cycle.

A block in G2-phase is a hallmark response to DNA damage. Therefore, we assessed markers of DNA damage at different stages of the cell cycle by flow cytometry (**Supplementary Fig. 4**). G0/G1 P1P2dKO pro-B cells are bigger compared to P1sKO and control G0/G1 pro-B cells (FSC-A measurements, **Supplementary Fig. 4a**). This is consistent with a predisposition to enter S-phase, as size increase and S-phase entry are positively correlated (Ginzberg et al., 2015). This increase in size resulted in higher intracellular background staining with isotype-control antibodies in G0/G1 P1P2dKO pro-B cells compared to G0/G1 P1sKO and control pro-B cells (**Supplementary Fig. 4b, c**). pH2AX staining in P1P2dKO pro-B cells was not increased compared to P1sKO and

control pro-B cells above the increase seen in background staining controls (**Supplementary Fig. 4b, c**). Staining of bone marrow cells treated with etoposide to induce DNA damage showed that P1P2dKO pro-B cells increased pH2AX levels to the same extent as P1sKO and control pro-B cells (**Supplementary Fig. 4d, e**). We found an increase (2.1-fold) in p53 staining in P1P2dKO G0/G1 pro-B cells compared to control G0/G1 pro-B cells above the increase (1.6-fold) seen in background staining controls (**Supplementary Fig. 4f, g**). Upon etoposide treatment, the fold increase in p53 in P1P2dKO G0/G1 pro-B cells compared to control pro-B cells (2.5-fold) was higher than in pro-B cells without etoposide treatment (2.1-fold) (**Supplementary Fig. 4g**). Thus, p53 levels provide some evidence of DNA damage in pro-B cells lacking PTBP1 and PTBP2 but these DNA damage levels are insufficient to be detected by pH2AX-staining. Therefore, DNA damage in P1P2dKO pro-B cells could contribute to the block in G2-phase.

PTBP1 is necessary to maintain transcriptome fidelity in pro-B cells

To identify the consequences of PTBP deficiency on the transcriptome of pro-B cells we carried out mRNAseq with polyadenylated transcripts from P1P2dKO, P1sKO and control cKIT^{+} pro-B (FrB) cells (**Supplementary Fig. 5**). To identify candidate transcripts directly bound and regulated by PTBP1 we made use of a PTBP1 individual-nucleotide resolution Cross-Linking and ImmunoPrecipitation (iCLIP) (König et al., 2010) dataset which reveals PTBP1-binding sites in the whole transcriptome and thereby allows distinction between direct and indirect targets. The PTBP1 iCLIP data was from mitogen-activated mouse primary B cells (Monzon-Casanova et al., 2018) because it was not feasible to purify sufficient numbers of pro-B cells for iCLIP. There is a positive correlation between the transcriptomes from mitogen-activated primary B cells and pro-

B cells (**Supplementary Fig. 6a**), suggesting that the available PTBP1 iCLIP data set (**Supplementary Tables 1, 2**) allows to infer direct interactions of PTBP1 in pro-B cells.

We analysed changes in mRNA abundance by comparing pro-B cell transcriptomes from the different genotypes in pairwise comparisons (**Fig. 3a**). There were more genes showing differential mRNA abundance when comparing P1P2dKO to control pro-B cells (1226 genes) and P1P2dKO to P1sKO pro-B cells (1202 genes) than when comparing P1sKO to control pro-B cells (214 genes) (using a $\log_2$-transformed fold change >|0.5| and FDR <0.05, **Supplementary Table 3**). We found that only ~25% of the genes with either increased or decreased mRNA abundance due to absence of both PTBP1 and PTBP2 were directly bound by PTBP1 at the 3'UTR and are therefore likely to be direct targets (**Supplementary Fig. 6b** and **Supplementary Table 3**). The remaining changes observed in mRNA abundance upon *Ptbp1* and *Ptbp2* deletion can be expected to be independent from a direct role of PTBP1 via 3'UTR binding. *Ptbp2* mRNA abundance was increased ~18-fold in P1sKO compared to control pro-B cells (**Fig. 3a, Supplementary Table 3**). Similarly, P1P2dKO pro-B cells showed an upregulation (~6.8-fold) of *Ptbp2* mRNA compared to control pro-B cells (**Fig. 3a**, middle plot). However, *Ptbp2* transcripts in P1P2dKO pro-B cells lack *Ptbp2* exon 4 due to the conditional knock-out (**Supplementary Fig. 6c**), and hence do not result in PTBP2 protein expression (**Supplementary Fig. 2b**).

We assessed alternative splicing (AS) differences in pro-B cells with different genotypes by computing differences in exon inclusion levels in pairwise comparisons with rMATS (Shen et al., 2014) (**Fig. 3b, Supplementary Table 4**). rMATS considers five different types of alternatively spliced events: skipped exons, mutually exclusive exons, alternative

5' and 3' splice sites (SS) and retained introns (**Supplementary Fig. 6d**). The inclusion level of a particular AS event is the proportion (scaled to 1) of transcripts containing the alternatively spliced mRNA segment. We chose a threshold of an absolute inclusion level difference >0.1 to identify substantial changes in AS. Similar to our observations in mRNA abundance, the absence of both PTBP1 and PTBP2 in pro-B cells resulted in more differentially alternatively spliced events (P1P2dKO – Ctrl, 1599 events in 1058 genes) than the absence of PTBP1 (P1sKO – Ctrl, 865 events in 659 genes) (**Fig. 3b**). Depending on the type of AS event analysed, from 30 to 50% of the events with changes in AS, when comparing P1P2dKO to control pro-B cells, were bound in their vicinity by PTBP1 (**Supplementary Fig. 6e, Supplementary Table 4**). This implicates PTBP1 in controlling these AS events directly. There is a small overlap of genes with changes in mRNA abundance and also AS in the different pairwise comparisons (**Fig. 3c**), indicating that the inclusion of certain exons may generate NMD targets. Such AS events promoting NMD are most likely underestimated, since the RNA containing these events will be degraded and it might be difficult to detect by mRNAseq.

As B cell development is largely unaffected in P1sKO mice we focused on differences in mRNA abundance and AS unique to P1P2dKO pro-B cells compared to both P1sKO and control pro-B cells to identify changes causing the developmental block in P1P2dKO mice. We identified 1021 and 611 genes with decreased and increased mRNA abundance, respectively, in P1P2dKO compared to control and P1sKO pro-B cells (**Fig. 3d**). Amongst AS changes, we found 971 genes with increased or decreased inclusion levels of at least one event in P1P2dKO pro-B cells compared to control and P1sKO (**Fig. 3e**). When addressing abundance changes, P1P2dKO pro-B cells cluster separately from P1sKO and control pro-B cells (**Fig. 3d**). In contrast, when analysing AS, P1P2dKO and P1sKO pro-B

cells cluster together and separately from control pro-B cells (**Fig. 3e**). Therefore, PTBP2 is more able to compensate for the absence of PTBP1 at the mRNA abundance than at the AS level. We observed only few genes with different mRNA abundance (cluster d) or changes in AS (clusters i and iii) that were predominantly regulated in P1sKO pro-B cells compared to P1P2dKO and control pro-B cells (**Fig. 3d, e**). In contrast, large numbers of genes had different mRNA abundance (clusters a, b and c) and AS (clusters ii and iv) in P1P2dKO pro-B cells compared to P1sKO and control pro-B cells (**Fig. 3d, e**). Therefore, in pro-B cells, PTBP2 has only few specific targets and mostly compensates for the absence of PTBP1. We conclude that in pro-B cells PTBP1 ensures appropriate expression at the level of AS and mRNA abundance level of more than 2000 genes and therefore promotes the fidelity of their transcriptome.

PTBP1 controls CDK activity in pro-B cells

To assess functions of the genes with altered expression in P1P2dKO pro-B cells we carried out gene ontology (GO) enrichment analysis on genes with increased or reduced abundance or with AS changes. We found numerous enriched GO terms important for the biology of B cells and their progenitors (**Fig. 4a, Supplementary Table 5**) such as "antigen processing and presentation of peptide antigen via MHC class II" amongst genes with increased abundance and "positive regulation of DNA-binding transcription factor activity" amongst genes with decreased abundance. We found enrichment of terms related to migration such as "neuronal crest migration" and "neutrophil migration". At the AS level, enrichment of the term "cytoskeletal protein binding" suggests PTBP1 as a cytoskeleton regulator. "Regulation of neuron differentiation" was enriched amongst genes with reduced abundance and with changes in AS, as we expected from the known roles of PTBPs in neuronal development (Hu et al., 2018). Thus, PTBP1 is necessary in

pro-B cells to promote adequate expression of many different pathways fundamental for cell biology.

In P1P2dKO pro-B cells there were no obvious expression defects in genes important for the progression from pro- to pre-B cells (**Supplementary Fig. 6f, Supplementary Tables 3, 4**). Therefore, we focused on understanding the molecular mechanisms driving uncontrolled entry into S-phase and increased frequencies of pro-B cells in G2-phase. We only found one GO term amongst those enriched to be directly associated with proliferation: "cyclin-dependent protein serine/threonine kinase inhibitor activity". This was unexpected given the documented changes in the transcriptome across different phases of the cell cycle (Giotti et al., 2018) and that FrB pro-B cells from which we carried out mRNAseq in P1P2dKO mice have a ~10% increase of cells in S-phase and ~12% increase of cells in G2/M-phase compared to control and P1sKO FrB pro-B cells (**Supplementary Fig. 3g, h**). Moreover, we did not find a global increase of S- and G2/M-associated transcripts (Giotti et al., 2018) in the P1P2dKO pro-B transcriptome (**Fig. 4b**). Instead, we found 8 genes with a reduction of mRNA abundance greater than 2-fold (<-1 Log_2-fold change) in P1P2dKO compared to control pro-B cells (**Supplementary Table 6**). This indicates that the majority of the changes observed in the transcriptome of P1P2dKO compared to control and P1sKO pro-B cells are not the result of comparing populations with different proliferative status, but are reflective of an altered pro-B cell transcriptome.

Amongst genes associated with "cyclin-dependent protein serine/threonine kinase inhibitor activity", we found reduced mRNA abundance in *Cdkn1b, Cdkn1c, Cdkn2c* and *Cdkn2d* (encoding p27, p57, p18 and p19, respectively) due to PTBP1 and PTBP2 absence

(**Fig. 5a**). None of these CDK inhibitors has an obvious change in AS or a binding site for PTBP1 in the 3'UTR (**Supplementary Tables 2, 4**). Therefore, the changes in mRNA expression of CDK inhibitors are likely to be indirectly regulated by PTBP1. We stained p27 protein across different phases of the cell cycle and found it to be reduced ~1.7-fold in G0/G1 P1P2dKO pro-B cells compared to G0/G1 P1sKO and control pro-B cells (**Fig. 5b, c**), consistent with the decreased mRNA abundance observed in mRNA-Seq (**Fig. 5a**). In contrast, p27 staining was increased ~7-fold in G2 P1P2dKO pro-B cells compared to P1sKO and control G2 pro-B cells (**Fig. 5b, c**). These differences in p27 staining seen between G0/G1 and G2 phases are consistent with an indirect role of PTBP1 in controlling p27 expression. In addition to p27 staining, we assessed CDK activity by measuring the extent of RB phosphorylation, which is started in G1 by CDKs and promotes the entry into S-phase (Otto and Sicinski, 2017). Almost all P1P2dKO G0/G1 pro-B cells had phosphorylated RB whereas only ~30% of P1sKO and control G0/G1 pro-B cells had phosphorylated RB (**Fig. 5d, e**), showing that P1P2dKO pro-B cells in G0/G1-phase have abnormally high CDK activity. In contrast, P1P2dKO pro-B cells in G2-phase had much lower proportions of cells with highly phosphorylated RB (~30%) compared to G2 P1sKO and control pro-B cells (~70%) (**Fig. 5d, e**). This suggests an impaired CDK activity amongst G2 P1P2dKO pro-B cells, consistent with high p27 levels. The phosphorylation of threonine-592 on SAMHD1 is mediated by CDK1 (Cribier et al., 2013). Proportions of phospho-T592-SAMHD1-positive cells amongst P1P2dKO G2 pro-B cells were reduced compared to P1sKO and control G2 pro-B cells (**Fig. 5d, e**). These results indicate a requirement of PTBPs to achieve the adequate CDK1 activity necessary to enter mitosis. Thus, PTBPs are essential for controlling activity of CDKs in different phases of the cell cycle in pro-B cells: to limit entry into S-phase and to promote progression through mitosis.

PTBP1 controls expression of a cell cycle mRNA regulon in pro-B cells

The changes in expression of CDK inhibitors seemed an indirect consequence of *Ptbp1* and *Ptbp2* deletion and cell cycle gene sets were not enriched amongst genes with altered mRNA expression in the P1P2dKO pro-B cells. Thus, instead of gene sets, it was possible that individual genes with rate limiting properties for cell cycle progression, which could also control the expression of CDK-inhibitors and CDK activities, were directly regulated by PTBP1. Therefore, we considered further genes affected in the absence of PTBP1 and PTBP2 but not in the absence of PTBP1 alone that are known to regulate the cell cycle (**Fig. 6**). We identified nine candidate targets with direct PTBP1 binding and changes at the levels of mRNA abundance and AS that constitute an mRNA regulon controlling the cell cycle.

We found three genes (*Foxo1*, *Btg2* and *Rbl1*) whose proteins inhibit S-phase entry with reduced mRNA abundance in P1P2dKO compared to control and P1sKO pro-B cells (**Fig. 6a**). Additionally, two genes whose proteins promote entry into S-phase (*Myc* and *Ccnd2*) showed increased mRNA abundance due to *Ptbp1* and *Ptbp2* deletion (**Fig. 6a**). FOXO transcription factors promote p27 expression and inhibit CDK activity (Herzog et al., 2009). PTBP1 bound to the 3'UTR of *Foxo1* (**Supplementary Fig. 7a**). No obvious change in *Foxo1* AS was detected upon *Ptbp1* and *Ptbp2* deletion (**Supplementary Table 4**). Therefore, PTBP1 expression enhances *Foxo1* mRNA abundance in pro-B cells. PTBP1 bound to *Myc* 3'UTR (**Supplementary Fig. 7a**). We confirmed an increase of c-MYC protein in G0/G1 P1P2dKO pro-B cells compared to control and P1sKO G0/G1 pro-B cells (**Supplementary Fig. 7b, c**) as the fold-change increase in fluorescence intensity of the c-MYC staining (2.2-fold) was greater than the fold-change increase in fluorescence

intensity of the control staining (1.5-fold). Therefore, in pro-B cells PTBP1 suppresses *Myc*. CYCLIN-D2 pairs with CDK4/6. *Ccnd2* abundance (encoding CYCLIN-D2) was increased ~2-fold in P1P2dKO compared to control and P1sKO pro-B cells (**Fig. 6a**) and PTBP1 bound to *Ccnd2* 3'UTR (**Supplementary Fig. 7a**). c-MYC induces transcription of *Ccnd2* (Bouchard et al., 2001). Therefore, PTBP1 and PTBP2 may reduce *Ccnd2* abundance indirectly by suppressing c-MYC-mediated transcription and directly by binding its mRNA. BTG2 inhibits G1 to S transition and promotes B cell development by suppressing proliferation in late-pre-B cells (Dolezal et al., 2017). *Btg2* mRNA abundance was reduced ~2-fold due to *Ptbp1* and *Ptbp2* deletion (**Fig. 6a**). No obvious change in *Btg2* AS was detected but PTBP1 binding sites were present at the *Btg2* 3'UTR (**Supplementary Fig. 7a**). Therefore, PTBP1 could directly promote BTG2 expression in pro-B cells by stabilising *Btg2* transcripts. p107 (encoded by *Rbl1*) represses E2F transcription factors and entry into S-phase (Bertoli et al., 2013). *Rbl1* mRNA abundance was reduced ~1.5-fold in P1P2dKO compared to control and P1sKO pro-B cells (**Fig. 6a**). PTBP1 and PTBP2 suppress the inclusion of a downstream alternative 5'SS (A5SS) in *Rbl1* exon 8 which generates an NMD-target isoform in P1P2dKO pro-B cells (**Fig. 6b**). PTBP1 binds to adjacent regions of this alternatively spliced event (**Fig. 6b**). This A5SS event is conserved in human, as PTBP1- and PTBP2-depleted HeLa cells (Ling et al., 2016) also have an increased usage of the downstream A5SS compared to PTBP-sufficient cells resulting in reduced *RBL1* mRNA abundance (**Fig. 6c, d**). Therefore, PTBP1 promotes *Rbl1* expression. Collectively, deregulated expression of *Foxo1*, *Myc*, *Ccnd2*, *Btg2* and *Rbl1* in the absence of PTBP1 and PTBP2 could drive entry of pro-B cells into S-phase.

We also found transcripts important for the transition from G2 to M-phase altered in P1P2dKO pro-B cells. The abundance of *Cdc25b*, *Ect2, Kif2c* and *Kif22* was reduced (~3,

~5, ~2 and ~2-fold, respectively) in P1P2dKO compared to control and P1sKO pro-B cells (**Fig. 6a**). CDC25B is a phosphatase promoting G2/M transition by activating CDK1 (Boutros et al., 2007). *Cdc25b* AS was unaffected by PTBP1 and PTBP2 absence and PTBP1 bound to the *Cdc25b* 3'UTR (**Supplementary Table 4** and **Supplementary Fig. 7a**). Thus, PTBP1 likely promotes *Cdc25b* expression by binding to its 3'UTR and enhancing its stability. Additionally, there were three genes where their changes in mRNA abundance can be explained by AS events leading to NMD. ECT2 controls spindle formation in mitosis by exchanging GDP for GTP in small GTPases such as RhoA (Yüce et al., 2005). In P1P2dKO pro-B cells *Ect2* has an increased inclusion of an alternative exon compared to P1sKO and control pro-B cells (**Fig. 6b**). Inclusion of this AS exon, using either of two alternative 3' splice sites, generates NMD-predicted transcripts. PTBP1 binds nearby this NMD-triggering exon where it is predicted to suppress exon inclusion (Llorian et al., 2010) promoting high *Ect2* mRNA levels in pro-B cells. KIF2c (MCAK) and KIF22 (KID) are two kinesin motor family members that transport cargo along microtubules during mitosis (Cross and McAinsh, 2014). Both have increased inclusion of an exon that generates predicted NMD-targets in P1P2dKO compared to P1sKO and control pro-B cells and some evidence for PTBP1 binding in adjacent regions (**Fig. 6b**). This data shows that PTBP1 promotes expression of genes important for mitosis by controlling AS linked to NMD. The altered expression of these genes in the absence of PTBP1 and PTBP2 is likely to contribute to the high proportions of G2 cells observed in P1P2dKO pro-B cells. Our findings place PTBP1 as a regulator of the cell cycle in pro-B cells. PTBP1 is essential to control appropriate expression of an mRNA regulon dictating CDK activity, progression to S-phase and entry into mitosis. In the absence of PTBP1 and its partially redundant paralog PTBP2, the molecular control of the cell cycle in primary pro-B cells is altered and B cell development is halted (**Fig. 6e**).

Discussion

Here we present an essential role for PTBP1 and PTBP2 in controlling B cell development and the proliferative status of pro-B cells. PTBP1 and PTBP2 deficiency in pro-B cells triggered entry into S-phase and accumulation in G2-phase, causing a complete block in B cell development. PTBP1 suppression of entry into S-phase was unanticipated since in other systems, including germinal centre (GC) B cells, PTBP1 promoted proliferation (Suckale et al., 2011; Shibayama et al., 2009; La Porta et al., 2016) and progression through late S-phase (Monzon-Casanova et al., 2018). GC B cells did not tolerate deletion of both PTBP1 and PTBP2 (Monzon-Casanova et al., 2018) and previous studies addressing proliferation in PTBP1-deficient cells were done in the presence of PTBP2 (Suckale et al., 2011; Shibayama et al., 2009; La Porta et al., 2016). Therefore, the role of PTBP1 in suppressing S-phase entry could be unique to pro-B cells or could be found in other cell types if they resist the absence of PTBP1 and PTBP2 long enough to assess cell-cycle progression.

Suppression of proliferation in pre-B cells is necessary to allow Igl recombination (Clark et al., 2014). Similarly, in pro-B cells entry into S-phase will inhibit VDJ Igh recombination. We have previously shown that the RNA-binding proteins ZFP36L1 and ZFP36L2 suppress proliferation in pro-B cells, facilitate Igh recombination and consequently promote B cell development (Galloway et al., 2016). In the absence of PTBP1 and PTBP2, expression of *Zfp36l1* was normal and *Zfp36l2* was increased ~1.5-fold (**Supplementary Table 3**), but still there was no suppression of S-phase entry. This suggests the presence of distinct mRNA regulons controlled by the different RBPs important to control cell cycle

entry. Our results reveal the importance of suppressing proliferation also in pro-B cells for successful B cell development.

PTBP1 maintains the fidelity of the transcriptome in pro-B cells since the absence of PTBP1 and PTBP2 caused changes in mRNA expression of 2000 genes. In particular, PTBP1 expression controls a cell cycle mRNA regulon comprising *Foxo1, Myc*, *Ccnd2*, *Btg2*, *Rbl1*, *Cdc25b*, *Ect2*, *Kif22* and *Kif2c*. Proteins from this mRNA regulon control each other and have downstream effects on other cell cycle regulators. FOXO proteins suppress D-type cyclins (Schmidt et al., 2002) and promote p27 (Herzog et al., 2009). c-MYC suppresses *Cdkn1b* (encoding p27) (Yang et al., 2001) and increases *Ccnd2* transcription (Bouchard et al., 2001). CYCLIN-D2 promotes nuclear export and degradation of p27 (Susaki et al., 2007) and p27 can directly inhibit CYCLIN-D-CDK4/6 complexes (Yoon et al., 2012). We found evidence for interaction of PTBP1 with these transcripts implicating a direct role of PTBP1. Future investigations are needed to assess which of the PTBP1-binding sites are functional and control mRNA expression. However, since these targets regulate each other it will be difficult to deconvolute direct from indirect effects of PTBP1 controlling this cell cycle mRNA regulon. The net outcome from deregulation of these transcripts in the absence of PTBP1 and PTBP2 is an enhanced CDK activity in G0/G1 pro-B cells that drives entry into S-phase and a reduced CDK activity amongst blocked G2 pro-B cells.

Myc mRNA and protein abundance was increased due to *Ptbp1* and *Ptbp2* deletion in pro-B cells and PTBP1 was bound to the *Myc* 3'UTR. In GC B cells lacking PTBP1 alone, part of the c-MYC-activated gene expression program initiated upon positive selection was reduced while c-MYC protein expression was unaffected (Monzon-Casanova et al., 2018).

PTBP2 is redundant with PTBP1 in GC B cells (Monzon-Casanova et al., 2018), therefore it is possible that c-MYC protein would be increased in GC B cells if both PTBP1 and PTBP2 are absent. We were unable to address this because we did not detect GC B cells lacking both PTBP1 and PTBP2 (Monzon-Casanova et al., 2018). Alternatively, PTBP1 could have distinct roles in controlling c-MYC and its gene expression programme in different cell types.

Deletion of *Ptbp1* and *Ptbp2* in pro-B cells resulted in a block in G2-phase. Since the number of pro-B cells did not accumulate in P1P2dKO mice, it is likely that P1P2dKO pro-B cells die after the block at G2-phase. We found increased p53 in pro-B cells deficient for PTBP1 and PTBP2, indicating that DNA damage in pro-B cells contributes to the G2 block, although we did not detect a DNA damage signature amongst GO enrichment analysis. DNA damage in P1P2dKO pro-B cells could happen due to the enhanced entry into S-phase as this causes replication stress (Zeman and Cimprich, 2013). Moreover, p27 promotes G2 arrest in response to DNA-damage (Cuadrado et al., 2009; Payne et al., 2008). Thus, the increased p27 levels found in P1P2dKO pro-B cells blocked at G2-phase could be a response to DNA damage. Increased p27 will inhibit CDK activity and promote G2 block (Yoon et al., 2012). PTBP1 promotes p27 IRES-mediated translation in human cells (Cho et al., 2005). The sequence in the human *CDKN1B* (encoding p27) 5'UTR-IRES is conserved in mouse. We did not find mouse PTBP1 bound to the *Cdkn1b* 5'UTR in our iCLIP data. However, a direct role of PTBP1 in promoting p27 translation could still be possible in pro-B cells and is consistent with a reduction in p27 in G0/G1 pro-B cells due to PTBP1 and PTBP2 absence. Nevertheless, we found increased p27 levels in G2 pro-B cells due to *Ptbp1* and *Ptbp2* deletion and this would be inconsistent with PTBP1 promoting p27 expression. Additionally, CDC25B reduction has been shown to cause a

G2 block (Peco et al., 2012; Lindqvist et al., 2005). Therefore, *Cdc25b* reduction in P1P2dKO pro-B cells, in addition to the other mechanisms discussed, could also contribute to the block in G2-phase.

Various RBPs promote transcriptome fidelity by suppressing non-conserved cryptic exons which in normal conditions should never be included and often generate NMD targets (Ling et al., 2016; Sibley et al., 2016). Cryptic exons suppressed by PTBP1 have been found when both PTBP1 and PTBP2 were depleted (Ling et al., 2016). These cryptic exons are poorly conserved between mouse and human. In pro-B cells deficient for PTBP1 and PTBP2 we found cryptic exons promoting mRNA degradation amongst cell cycle regulators. For most of them we did not find evidence for their conservation in human cells where PTBP1 and PTBP2 were absent (Ling et al., 2016). However, the A5SS in *Rbl1* generating an NMD-target was conserved in human, suggesting that it is a functional AS-NMD event with a role in post-transcriptional control. Altogether, PTBP1 expression in pro-B cells controls correct expression of thousands of genes. In particular, PTBP1 controls a network of factors essential to avoid S-phase entry followed by a G2 block and to promote B cell development beyond the pro-B cell stage.

Methods

Mice

Mice were bred and maintained in the Babraham Institute Biological Support Unit under Specific Opportunistic Pathogen Free (SOPF) conditions. After weaning, mice were transferred to individually ventilated cages with 1-5 mice per cage. All experiments were carried out without blinding or randomization on 7 to 15-week-old mice. Conditional knockout mice used were derived from crossing the following transgenic strains: *Ptbp1*$^{fl/fl}$(Ptbp1^{tm1Msol}) (Suckale et al., 2011), *Ptbp2*$^{fl/fl}$(Ptbp2$^{tm1.1Dblk}$) (Li et al., 2014) and *Cd79a*^{cre}(Cd79a$^{tm1(cre)Reth}$) (Hobeika et al., 2006). *Rag2*$^{-/-}$ knockout mice (Shinkai et al., 1992) (Rag2^{tm1Fwa}) were also used. All mice were on a C57BL/6 background.

In vivo EdU and BrdU administration

All procedures performed were approved by the Babraham Institute's Animal Welfare and Experimentation Committee and the UK Home Office and followed all relevant ethical regulations. In EdU-only and in EdU and BrdU double-labelling experiments 1 to 5 mice of different genotypes and the same sex were kept in individually ventilated cages. Whenever possible females were used as this allowed for a higher number of mice with different genotypes per cage. Males and females showed the same differences in the phenotypes observed due to PTBPs absence. In Edu-only labelling experiments mice were injected with 1 mg EdU (5-ethynyl-2'-deoxyuridine, cat #E10415, ThermoFisher Scientific) was injected intraperitoneally and mice were culled one hour after injection. In EdU and BrdU (5-Bromo-2′-deoxyuridine, cat# B5002-500mg, Sigma) labelling experiments mice were injected first with 1 mg EdU (cat #E10415, ThermoFisher

Scientific) intraperitoneally, one hour later, the same mice were injected with 2 mg BrdU and the mice were culled 1 hour and 40 minutes after the injection with EdU.

Flow cytometry

Single cell suspensions were prepared from spleens and lymph nodes by passing the organs through cell strainers with 70 µm and 40 µm pore sizes in cold RPMI-1640 (cat# R8758, Sigma) with 2% fetal calf serum (FCS). Single cell suspensions from bone marrows were prepared by flushing the bone marrow from femurs and tibias and passing the cells through a cell strainer with 40 µm pore size in cold RPMI-1640 with 2%FCS. Fc receptors were blocked with monoclonal rat antibody 2.4G2. Cells were stained with combinations of antibodies listed in **Supplementary Table 7**. Cell surface staining was carried out for 45 minutes on ice by incubating cells with a mixture of antibodies in cold FACS buffer (PBS +0.5%FCS). For intracellular staining cells were fixed with Cytofix/Cytoperm™ Fixation and Permeabilization Solution (cat# 554722, BD) on ice, washed with FACS Buffer and frozen in 10% DMSO 90% FCS at -80°C at least overnight. After thawing, cells were washed with FACS Buffer and re-fixed with Cytofix/Cytoperm™ Fixation and Permeabilization Solution (cat# 554722, BD) for 5 minutes on ice. Cells were washed with Perm/Wash Buffer (cat# 554723, BD) and intracellular staining with antibodies were carried out by incubating first fixed and permeabilized cells in Perm/Wash Buffer (cat# 554723, BD) with monoclonal rat antibody 2.4G2 and subsequently with the desired antibodies in Perm/Wash Buffer at room temperature. EdU was detected with Click-iT™ Plus EdU kits (cat# C10646, for AF594 and cat# C10636 for pacific blue, ThermoFisher Scientific). For double detection of EdU and BrdU, cells were treated as for intracellular staining, but before adding the intracellular antibodies, cells were treated with TURBO™ DNase (12 units/10^7 cells, cat# AM2239,

ThermoFisher Scientific) for 1 hour at 37°C, subsequently, EdU was detected with the Click-iT™ reaction following the instructions from the manufacturer, cells were washed with Perm/Wash Buffer (cat# 554723, BD) and incubated with anti-BrdU-AF647 antibody (MoBU-1, cat# B35133, ThermoFisher Scientific). DNA was stained in the last step before flow cytometry analysis with 7AAD in EdU and BrdU double-labelling experiments or with Vybrant™ DyeCycle™ Violet Stain in experiments where no DNA-digestion was carried out (cat # V35003, ThermoFisher Scientific). In experiments where cells were treated with etoposide to induce DNA damage, single cell suspensions from bone marrow were incubated with 20μM etoposide (cat# E1383-100MG, Sigma) in RPMI +2%FCS for 3 hours at 37°C. Flow cytometry data was acquired on a BD LSRFortessa with 5 lasers and was analysed using FlowJo software (versions 10.6.0 and 10.0.8r1).

mRNAseq libraries from FrB pro-B cells

FrB c-KIT+ pro-B cells (B220^{+}, CD19^{+}, IgD^{-}, IgM^{-}, CD2^{-}, CD25^{-}, CD43^{high}, cKIT^{+}, CD24^{+} and CD249^{-}) were sorted from bone marrow cells isolated from femurs and tibias. Bone marrow cells from 4-6 mice from the same genotype and sex were pooled and depleted of unwanted cells with anti Gr-1-bio (RB6-8C5), CD11b (M1/70), IgD-bio (11-26c.2a), NK1.1-bio, CD3e (145-2C11) and Ter119 biotinylated antibodies and anti-biotin microbeads (cat# 130-090-485, Miltenyi) before sorting. Sorting strategy of FrB pro-B cells is shown in **Supplementary Fig. 5**. RNA from 15,000 to 200,000 FrB cells was isolated with the RNeasy Micro Kit (cat# 74004, Qiagen). mRNAseq libraries from 5 biological replicates per genotype: (three genotypes: ctrl (*Cd79a*$^{+/+}$*Ptbp1*$^{fl/fl}$*Ptbp2*$^{fl/fl}$), P1sKO (*Cd79a*$^{cre/+}$*Ptbp1*$^{fl/fl}$*Ptbp2*$^{+/+}$) and P1P2dKO (*Cd79a*$^{cre/+}$*Ptbp1*$^{fl/fl}$*Ptbp2*$^{fl/fl}$); three samples from females and two samples from males per genotype) were prepared by generating cDNA from 2 ng RNA and 9 PCR cycles per replicate with the SMART-Seq® v4

Ultra® Low Input RNA Kit for Sequencing (cat# 634891, Takara) and by enzymatic fragmentation of 300 pg of cDNA followed by 12 PCR cycles using the Nextera XT DNA Library Preparation Kit (cat# FC-131-1096, Illumina). Sequencing of the 15 mRNAseq libraries multiplexed together was carried out with an Illumina HiSeq2500 on a 2x125 bp paired-end run.

PTBP1 iCLIP

PTBP1 iCLIP was carried out previously from mitogen-activated B cells (splenic B cells stimulated with LPS for 48 hours)(Monzon-Casanova et al., 2018). This data was re-analysed to map reads using a splicing-aware software. Reads from five PTBP1 iCLIP libraries were mapped to the GRCm38.p5 mouse genome from Gencode with STAR (v 2.5.4b)(Dobin et al., 2013). Reads were de-duplicated using random barcodes included in the library preparation and xlink-sites (**Supplementary Table 1**) and clusters of binding (**Supplementary Table 2**) were identified with iCount https://icount.readthedocs.io/en/latest/cite.html as previously described(Monzon-Casanova et al., 2018). Detection of a binding site with iCLIP(König et al., 2010) is highly dependent on the abundance of the RNA, therefore all replicates were pooled together to identify xlink sites and clusters of binding. Xlink sites and clusters of PTBP1 binding were assigned to transcripts and genomic features with the following hierarchy: CDS, 3'UTR, 5'UTR, intron, ncRNA using the Mus_musculus.GRCm38.93.gtf annotation from Ensembl (**Supplementary Tables 1, 2**)

mRNA abundance analysis

mRNAseq libraries were trimmed with Trim Galore (v 1.15 https://www.bioinformatics.babraham.ac.uk/projects/trim_galore/) with default

parameters and mapped with Hisat2 (v 2.1.0) (Kim et al., 2015) with -p 7 -t --phred33-quals --no-mixed --no-discordant parameters, the Mus_musculus.GRCm38 genome and known splice sites from the Mus_musculus.GRCm38.90 annotation. Read counts mapped over genes were counted with HTSeq (v0.10.0) (Anders et al., 2015) with f bam -r name -s no -a 10 parameters and the Mus_musculus.GRCm38.93.gtf annotation from Ensembl. Reads mapping to immunoglobulin genes (including V, D, J gene segments, light and heavy immunoglobulin genes and T cell receptor genes) were excluded before DESeq2 analysis. Differences in mRNA abundance were computed with DESeq2 (v1.22.1) (Love et al., 2014) by extracting differences between different genotypes in pair-wise comparisons using "apeglm" method as a shrinkage estimator (Zhu et al., 2019). Information on the sex of the mice from which the mRNAseq libraries were generated was included in the design formula in addition to the genotype (design = ~ Sex + Genotype). From the DESeq2 results we only considered genes with a mean expression level of at least 1 FPKM (from the five biological replicates) in any of the three genotypes analysed. FPKMs were calculated with cuffnorm from Cufflinks (v2.2.1) (Trapnell et al., 2012) using the -library-norm-method geometric. We considered genes with differential mRNA abundance as those with a log2-fold change >|0.5| and a p-adjusted value of <0.05 (**Supplementary Table 3**).

A gene with different mRNA abundance was bound by PTBP1 at the 3'UTR if at least one cluster of PTBP1-binding from the PTBP1 iCLIP data (**Supplementary Table 2**) was found to overlap with any 3'UTRs annotated in the Mus_musculus.GRCm38.93.gtf for that gene after assignation to genomic features for the binding sites of the iCLIP as described above.

Genes with different mRNA abundance in P1P2dKO FrB pro-B cells compared to P1sKO and control FrB cells (**Fig. 3d, Supplementary Table 5**) were identified after hierarchical clustering of the Euclidian distances between Z-scores of each gene calculated from the DESeq2 normalised read counts for the 15 mRNAseq libraries (5 biological replicates per genotype). Genes with different mRNA abundance in any of the three pairwise comparisons carried out (**Fig. 3a**) were considered in the hierarchical clustering.

Alternative splicing analysis

Trimmed reads with Trim Galore were further trimmed to 123 bp and reads which were smaller than 123 bp were discarded with Trimmomatic (v0.35) (Bolger et al., 2014) in order to obtain only pairs of reads 123 bp long. 123 bp-long reads were mapped to the Mus_musculus.GRCm38 genome as described above, but only uniquely-mapped reads were kept by using the -bS -F 4 -F 8 -F 256 -q 20 parameters in samtools when converting hisat2 sam files to bam files. rMATS (Turbo v4.0.2) (Shen et al., 2014) was run with the -t paired --readLength 123 parameters and the Mus_musculus.GRCm38.93.gtf annotation for each individual pairwise comparison. Only results from rMATS with reads on exon-exon junctions were considered further. Significantly differentially alternatively spliced events (**Supplementary Table 4**) were defined as events that have an FDR<0.05, have an absolute inclusion level difference >0.1, come from genes expressed with at least 1 FPKM (mean across five biological replicates in any of the genotypes analysed) and have at least 80 reads from the sum of the five biological replicates mapping to either the included or skipped alternatively spliced event in at least one of the two conditions analysed. Only alternatively spliced events with the highest inclusion level difference

were kept from AS events with had the same genomic coordinates in the AS event (**Supplementary Table 4**).

Proportions of differentially alternatively spliced events were defined as bound by PTBP1 (**Supplementary Fig. 6e, Supplementary Table 4**) with different rules depending on the type of AS event. An SE was bound by PTBP1 if PTBP1 clusters (**Supplementary Table 2**) were found on the SE, 500 nucleotides upstream or downstream of the AS SE, on either of the constitutive flanking exons or in 500 nucleotides downstream or upstream of the upstream and downstream constitutive exons, respectively. An A5SS was bound if PTBP1 clusters were found on the longest exon containing the A5SS, on the downstream intronic 500 nucleotides of the A5SS, on the downstream constitutive flanking exon or the 500 intronic nucleotides upstream of the downstream constitute flanking exon. An A3SS was bound by PTBP1 if PTBP1 clusters were found on the longest exon containing the A3SS, the 500 intronic nucleotides upstream of the A3SS, the upstream constitutive flanking exon or the 500 intronic nucleotides downstream of the upstream constitutive flanking exon. A MXE was bound by PTBP1 if PTBP1 clusters were found on either MXE, the upstream or downstream 500 intronic nucleotides of either MXE, the upstream or downstream constitutive flanking exons or the downstream or upstream 500 intronic nucleotides from the upstream or downstream constitutive flanking exons, respectively. A RI was bound by PTBP1 if PTBP1 clusters were found on the RI or on either constitutive flanking exon.

Events differentially alternatively spliced in P1P2dKO FrB pro-B cells compared to control and P1sKO FrB pro-B cells (**Fig. 3e**) were identified by hierarchical clustering using complete linkage clustering of the Euclidean distances between Z-scores of each AS

event calculated from the rMATS inclusion levels for the 15 mRNAseq libraries (5 biological replicates per genotype). AS events found in any of the three pairwise comparisons (**Fig. 3b**) were used in the hierarchical clustering.

Gene ontology term enrichment analysis

Genes belonging to different clusters based on differences in mRNA abundance or AS patterns between the P1P2dKO FrB pro B cells and the other genotypes (P1sKO and Controls) (**Fig. 3e, d** and **Supplementary Table 5**) were used for gene ontology enrichment analysis with GOrilla (Eden et al., 2009). Genes expressed with a mean of least 1 FPKM across the 5 biological replicates in any of the genotypes were used as background list for expressed genes in FrB pro-B cells. **Fig. 4a** shows representative enriched terms selected amongst closely related GO terms by manual inspection of the ontology. **Supplementary Table 5** is a full list of all enriched gene ontology enriched terms. Representative selected terms are highlighted.

Comparison of transcriptomes from pro-B cells and mitogen activated B cells

Transcriptomes from control FrB pro-B cells and mitogen activated primary B cells (LPS for 48 hours) (Diaz-Muñoz et al., 2015) were compared by calculating Spearman's rank correlation of the Log mean TPM (Transcripts per million reads) for each gene. Mean TPMs were calculated in FrB pro-B cells from five biological replicates and in mitogen-activated B cells from four biological replicates. TPMs were calculated after counting reads mapping to genes with HTSeq and the Mus_musculus.GRCm38.93.gtf annotation from Ensembl.

mRNAseq from human PTBP1 and PTBP2 depleted HeLa

Control and mRNAseq libraries where PTBP1 and PTBP2 were knocked down in HeLa cells by Ling et al. (Ling et al., 2016) were trimmed with Trim Galore (v 0.6.2_dev) and mapped with Hisat2 (v 2.1.0) (Kim et al., 2015) with --dta --sp 1000,1000 -p 7 -t --phred33-quals --no-mixed --no-discordant parameters, the Homo_sapiens.GRCh38 genome annotation and a file with known splice sites generated from the Homo_sapiens.GRCh38.87 annotation. Mapped reads were counted with HTSeq (v0.10.0)(Anders et al., 2015) with -f bam -r name -s no -a 10 parameters and the Homo_sapiens.GRCh38.93.gtf annotation from Ensembl. Read counts were normalised with DESeq2 (Love et al., 2014) (v 1.20.0).

Statistical analysis

Statistical analysis of flow cytometry data was carried out with GraphPad Prism version 7.0e. Details of tests carried out are found in the legends. Statistical analysis of mRNAseq data was carried out as described in the mRNA abundance analysis and Alternative splicing analysis sections.

Data availability

mRNAseq libraries and iCLIP analysis generated in this study have been deposited in GEO and can be accessed with the GSE136882 accession code at GEO. Mitogen activated primary B cell mRNAseq libraries were previously reported and can be accessed with the GSM1520115, GSM1520116, GSM1520117and GSM1520118 accession codes in GEO.

Author contributions

E.M.C., M.T. and C.W.J.S. designed experiments. E.M.C. and K.T. performed experiments and analysed data. E.MC., L.S.M. and K.Z. designed and carried out computational analysis. E.M.C. and M.T. wrote the manuscript with input from the co-authors.

Acknowledgments

We thank Douglas L. Black for the *Ptbp2*$^{fl/fl}$ mice, Michael Reth for the *Cd79a*^{cre} mice, Frederick W. Alt for the *Rag2*$^{-/-}$ mice and Michele Solimena for the *Ptbp1*$^{fl/fl}$ mice and the anti-PTBP2 antibody; Kirsty Bates, Arthur Davis, Attila Bebes, Simon Andrews, the Biological Support Unit, Flow Cytometry and Bioinformatics Facilities for technical assistance; Tony Ly, Anne Corcoran and members of the Turner, Smith and Zarnack laboratories for helpful discussions. This study was supported by funding from the Biotechnology and Biological Sciences Research Council (BB/J00152X/1; BB/P01898X/1; BBS/E/B/000C0407; and BBS/E/B/000C0427 and the Campus Capability Core Grant to the Babraham Institute), a Wellcome Investigator award to M.T and a Sort Term Scientific Mission Award to E.M.C. from the European Cooperation in Science and Technology action CA17103, Delivery of Antisense RNA Therapeutics. The authors declare no competing financial interests.

References

Anders, S., P.T. Pyl, and W. Huber. 2015. HTSeq--a Python framework to work with high-throughput sequencing data. *Bioinformatics*. 31:166–169. doi:10.1093/bioinformatics/btu638.

Bertoli, C., J.M. Skotheim, and R.A.M. de Bruin. 2013. Control of cell cycle transcription during G1 and S phases. *Nature Reviews Molecular Cell Biology*. 14:518–528. doi:10.1038/nrm3629.

Bolger, A.M., M. Lohse, and B. Usadel. 2014. Trimmomatic: a flexible trimmer for Illumina sequence data. *Bioinformatics*. 30:2114–2120. doi:10.1093/bioinformatics/btu170.

Bouchard, C., O. Dittrich, A. Kiermaier, K. Dohmann, A. Menkel, M. Eilers, and B. Lüscher. 2001. Regulation of cyclin D2 gene expression by the Myc/Max/Mad network: Myc-dependent TRRAP recruitment and histone acetylation at the cyclin D2 promoter. *Genes Dev.* 15:2042–2047. doi:10.1101/gad.907901.

Boutros, R., V. Lobjois, and B. Ducommun. 2007. CDC25 phosphatases in cancer cells: key players? Good targets? *Nature Reviews Cancer 2017 17:2*. 7:495–507. doi:10.1038/nrc2169.

Boutz, P.L., P. Stoilov, Q. Li, C.-H. Lin, G. Chawla, K. Ostrow, L. Shiue, M. Ares, and D.L. Black. 2007. A post-transcriptional regulatory switch in polypyrimidine tract-binding proteins reprograms alternative splicing in developing neurons. *Genes Dev.* 21:1636–1652. doi:10.1101/gad.1558107.

Busslinger, M. 2004. Transcriptional Control of Early B Cell Development1. *http://dx.doi.org/10.1146/annurev.immunol.22.012703.104807*. 22:55–79. doi:10.1146/annurev.immunol.22.012703.104807.

Cho, S., J.H. Kim, S.H. Back, and S.K. Jang. 2005. Polypyrimidine Tract-Binding Protein Enhances the Internal Ribosomal Entry Site-Dependent Translation of p27Kip1 mRNA and Modulates Transition from G1 to S Phase. *Mol. Cell. Biol.* 25:1283–1297. doi:10.1128/MCB.25.4.1283-1297.2005.

Clark, M.R., M. Mandal, K. Ochiai, and H. Singh. 2014. Orchestrating B cell lymphopoiesis through interplay of IL-7 receptor and pre-B cell receptor signalling. *Nature Reviews Immunology*. 14:69–80. doi:10.1038/nri3570.

Cribier, A., B. Descours, A.L.C. Valadão, N. Laguette, and M. Benkirane. 2013. Phosphorylation of SAMHD1 by Cyclin A2/CDK1 Regulates Its Restriction Activity toward HIV-1. *Cell Reports*. 3:1036–1043. doi:10.1016/j.celrep.2013.03.017.

Cross, R.A., and A. McAinsh. 2014. Prime movers: the mechanochemistry of mitotic kinesins. *Nature Reviews Molecular Cell Biology*. 15:257–271. doi:10.1038/nrm3768.

Cuadrado, M., P. Gutierrez-Martinez, A. Swat, A.R. Nebreda, and O. Fernandez-Capetillo. 2009. p27Kip1 Stabilization Is Essential for the Maintenance of Cell Cycle Arrest in

Response to DNA Damage. *Cancer Res.* 69:8726–8732. doi:10.1158/0008-5472.CAN-09-0729.

Diaz-Muñoz, M.D., S.E. Bell, K. Fairfax, E. Monzon-Casanova, A.F. Cunningham, M. Gonzalez-Porta, S.R. Andrews, V.I. Bunik, K. Zarnack, T. Curk, W.A. Heggermont, S. Heymans, G.E. Gibson, D.L. Kontoyiannis, J. Ule, and M. Turner. 2015. The RNA-binding protein HuR is essential for the B cell antibody response. *Nat. Immunol.* 16:415–425. doi:10.1038/ni.3115.

Dobin, A., C.A. Davis, F. Schlesinger, J. Drenkow, C. Zaleski, S. Jha, P. Batut, M. Chaisson, and T.R. Gingeras. 2013. STAR: ultrafast universal RNA-seq aligner. *Bioinformatics*. 29:15–21. doi:10.1093/bioinformatics/bts635.

Dolezal, E., S. Infantino, F. Drepper, T. Börsig, A. Singh, T. Wossning, G.J. Fiala, S. Minguet, B. Warscheid, D.M. Tarlinton, H. Jumaa, D. Medgyesi, and M. Reth. 2017. The BTG2-PRMT1 module limits pre-B cell expansion by regulating the CDK4-Cyclin-D3 complex. *Nat. Immunol.* 18:911–920. doi:10.1038/ni.3774.

Eden, E., R. Navon, I. Steinfeld, D. Lipson, and Z. Yakhini. 2009. GOrilla: a tool for discovery and visualization of enriched GO terms in ranked gene lists. *BMC Bioinformatics*. 10:48. doi:10.1186/1471-2105-10-48.

Galloway, A., A. Saveliev, S. Łukasiak, D.J. Hodson, D. Bolland, K. Balmanno, H. Ahlfors, E. Monzon-Casanova, S.C. Mannurita, L.S. Bell, S. Andrews, M.D. Diaz-Muñoz, S.J. Cook, A. Corcoran, and M. Turner. 2016. RNA-binding proteins ZFP36L1 and ZFP36L2 promote cell quiescence. *Science*. 352:453–459. doi:10.1126/science.aad5978.

Galloway, A., and M. Turner. 2017. Cell cycle RNA regulons coordinating early lymphocyte development. *Wiley Interdisciplinary Reviews: RNA*. 8:e1419. doi:10.1002/wrna.1419.

Ginzberg, M.B., R. Kafri, and M. Kirschner. 2015. On being the right (cell) size. *Science*. 348:1245075–1245075. doi:10.1126/science.1245075.

Giotti, B., S.-H. Chen, M.W. Barnett, T. Regan, T. Ly, S. Wiemann, D.A. Hume, and T.C. Freeman. 2018. Assembly of a Parts List of the Human Mitotic Cell Cycle Machinery. *J Mol Cell Biol*. 32:2858. doi:10.1093/jmcb/mjy063.

Hardy, R.R., and K. Hayakawa. 2003. B Cell Development Pathways. *https://doi.org/10.1146/annurev.immunol.19.1.595*. 19:595–621. doi:10.1146/annurev.immunol.19.1.595.

Hardy, R.R., C.E. Carmack, S.A. Shinton, J.D. Kemp, and K. Hayakawa. 1991. Resolution and characterization of pro-B and pre-pro-B cell stages in normal mouse bone marrow. *Journal of Experimental Medicine*. 173:1213–1225. doi:10.1084/jem.173.5.1213.

Herzog, S., M. Reth, and H. Jumaa. 2009. Regulation of B-cell proliferation and differentiation by pre-B-cell receptor signalling. *Nature Reviews Immunology*. 9:195–205. doi:10.1038/nri2491.

Hobeika, E., S. Thiemann, B. Storch, H. Jumaa, P.J. Nielsen, R. Pelanda, and M. Reth. 2006. Testing gene function early in the B cell lineage in mb1-cre mice. *PNAS*. 103:13789–13794. doi:10.1073/pnas.0605944103.

Hu, J., H. Qian, Y. Xue, and X.-D. Fu. 2018. PTB/nPTB: master regulators of neuronal fate in mammals. *Biophys Rep*. 4:204–214. doi:10.1007/s41048-018-0066-y.

Johnson, K., J. Chaumeil, M. Micsinai, J.M.H. Wang, L.B. Ramsey, G.V. Baracho, R.C. Rickert, F. Strino, Y. Kluger, M.A. Farrar, and J.A. Skok. 2012. IL-7 Functionally Segregates the Pro-B Cell Stage by Regulating Transcription of Recombination Mediators across Cell Cycle. *The Journal of Immunology*. 188:6084–6092. doi:10.4049/jimmunol.1200368.

Keene, J.D. 2007. RNA regulons: coordination of post-transcriptional events. *Nature Reviews Genetics 2013 14:7*. 8:533–543. doi:10.1038/nrg2111.

Kim, D., Ben Langmead, and S.L. Salzberg. 2015. HISAT: a fast spliced aligner with low memory requirements. *Nat. Methods*. 12:357–360. doi:10.1038/nmeth.3317.

Knoch, K.-P., H. Bergert, B. Borgonovo, H.-D. Saeger, A. Altkrüger, P. Verkade, and M. Solimena. 2004. Polypyrimidine tract-binding protein promotes insulin secretory granule biogenesis. *Nature Cell Biology*. 6:207–214. doi:10.1038/ncb1099.

Knoch, K.-P., S. Nath-Sain, A. Petzold, H. Schneider, M. Beck, C. Wegbrod, A. S nmez, C. M nster, A. Friedrich, M. Roivainen, and M. Solimena. 2014. PTBP1 is required for glucose-stimulated cap-independent translation of insulin granule proteins and Coxsackieviruses in beta cells. *Molecular Metabolism*. 3:518–530.

König, J., K. Zarnack, G. Rot, T. Curk, M. Kayikci, B. Zupan, D.J. Turner, N.M. Luscombe, and J. Ule. 2010. iCLIP reveals the function of hnRNP particles in splicing at individual nucleotide resolution. *Nat. Struct. Mol. Biol.* 17:909–915. doi:10.1038/nsmb.1838.

La Porta, J., R. Matus-Nicodemos, A. Valentín-Acevedo, and L.R. Covey. 2016. The RNA-Binding Protein, Polypyrimidine Tract-Binding Protein 1 (PTBP1) Is a Key Regulator of CD4 T Cell Activation. *PLoS ONE*. 11:e0158708. doi:10.1371/journal.pone.0158708.

Li, Q., S. Zheng, A. Han, C.-H. Lin, P. Stoilov, X.-D. Fu, D.L. Black, and B.J. Blencowe. 2014. The splicing regulator PTBP2 controls a program of embryonic splicing required for neuronal maturation. *eLife Sciences*. 3:e01201. doi:10.7554/eLife.01201.

Li, Z., D.I. Dordai, J. Lee, and S. Desiderio. 1996. A Conserved Degradation Signal Regulates RAG-2 Accumulation during Cell Division and Links V(D)J Recombination to the Cell Cycle. *Immunity*. 5:575–589. doi:10.1016/S1074-7613(00)80272-1.

Lindqvist, A., H. Källström, A. Lundgren, E. Barsoum, and C.K. Rosenthal. 2005. Cdc25B cooperates with Cdc25A to induce mitosis but has a unique role in activating cyclin B1–Cdk1 at the centrosome. *The Journal of Cell Biology*. 171:35–45. doi:10.1083/jcb.200503066.

Ling, J.P., R. Chhabra, J.D. Merran, P.M. Schaughency, S.J. Wheelan, J.L. Corden, and P.C. Wong. 2016. PTBP1 and PTBP2 Repress Nonconserved Cryptic Exons. *Cell Reports*. 17:104–113. doi:10.1016/j.celrep.2016.08.071.

Llorian, M., S. Schwartz, T.A. Clark, D. Hollander, L.-Y. Tan, R. Spellman, A. Gordon, A.C. Schweitzer, P. de la Grange, G. Ast, and C.W.J. Smith. 2010. Position-dependent alternative splicing activity revealed by global profiling of alternative splicing events regulated by PTB. *Nat. Struct. Mol. Biol.* 17:1114–1123. doi:10.1038/nsmb.1881.

Love, M.I., W. Huber, and S. Anders. 2014. Moderated estimation of fold change and dispersion for RNA-seq data with DESeq2. 15:550. doi:10.1186/s13059-014-0550-8.

Lu, R., K.L. Medina, D.W. Lancki, and H. Singh. 2003. IRF-4,8 orchestrate the pre-B-to-B transition in lymphocyte development. *Genes Dev.* 17:1703–1708. doi:10.1101/gad.1104803.

Ma, S., S. Pathak, M. Mandal, L. Trinh, M.R. Clark, and R. Lu. 2010. Ikaros and Aiolos Inhibit Pre-B-Cell Proliferation by Directly Suppressing c-Myc Expression. *Mol. Cell. Biol.* 30:4149–4158. doi:10.1128/MCB.00224-10.

Mandal, M., S.E. Powers, K. Ochiai, K. Georgopoulos, B.L. Kee, H. Singh, and M.R. Clark. 2009. Ras orchestrates exit from the cell cycle and light-chain recombination during early B cell development. *Nat. Immunol.* 10:1110–1117. doi:10.1038/ni.1785.

Monzon-Casanova, E., M. Screen, M.D. Diaz-Muñoz, R.M.R. Coulson, S.E. Bell, G. Lamers, M. Solimena, C.W.J. Smith, and M. Turner. 2018. The RNA-binding protein PTBP1 is necessary for B cell selection in germinal centers. *Nat. Immunol.* 45:471. doi:10.1038/s41590-017-0035-5.

Nahar, R., P. Ramezani-Rad, M. Mossner, C. Duy, L. Cerchietti, H. Geng, S. Dovat, H. Jumaa, B.H. Ye, A. Melnick, and M. Müschen. 2011. Pre-B cell receptor–mediated activation of BCL6 induces pre-B cell quiescence through transcriptional repression of MYC. *Blood*. 118:4174–4178. doi:10.1182/blood-2011-01-331181.

Otto, T., and P. Sicinski. 2017. Cell cycle proteins as promising targets in cancer therapy. *Nature Reviews Cancer 2017 17:2*. 17:93–115. doi:10.1038/nrc.2016.138.

Payne, S.R., S. Zhang, K. Tsuchiya, R. Moser, K.E. Gurley, G. Longton, J. deBoer, and C.J. Kemp. 2008. p27kip1 Deficiency Impairs G2/M Arrest in Response to DNA Damage, Leading to an Increase in Genetic Instability. *Mol. Cell. Biol.* 28:258–268. doi:10.1128/MCB.01536-07.

Peco, E., T. Escude, E. Agius, V. Sabado, F. Medevielle, B. Ducommun, and F. Pituello. 2012. The CDC25B phosphatase shortens the G2 phase of neural progenitors and promotes efficient neuron production. *Development*. 139:1095–1104. doi:10.1242/dev.068569.

Sasanuma, H., M. Ozawa, and N. Yoshida. 2019. RNA-binding protein Ptbp1 is essential for BCR-mediated antibody production. *Int. Immunol.* 31:157–166. doi:10.1093/intimm/dxy077.

Schlissel, M., A. Constantinescu, T. Morrow, M. Baxter, and A. Peng. 1993. Double-strand signal sequence breaks in V(D)J recombination are blunt, 5'-phosphorylated, RAG-dependent, and cell cycle regulated. *Genes Dev.* 7:2520–2532. doi:10.1101/gad.7.12b.2520.

Schmidt, M., S.F. de Mattos, A. van der Horst, R. Klompmaker, G.J.P.L. Kops, E.W.-F. Lam, B.M.T. Burgering, and R.H. Medema. 2002. Cell Cycle Inhibition by FoxO Forkhead Transcription Factors Involves Downregulation of Cyclin D. *Mol. Cell. Biol.* 22:7842–7852. doi:10.1128/MCB.22.22.7842-7852.2002.

Shen, S., J.W. Park, Z.-X. Lu, L. Lin, M.D. Henry, Y.N. Wu, Q. Zhou, and Y. Xing. 2014. rMATS: robust and flexible detection of differential alternative splicing from replicate RNA-Seq data. *Proc. Natl. Acad. Sci. U.S.A.* 111:E5593–601. doi:10.1073/pnas.1419161111.

Shibayama, M., S. Ohno, T. Osaka, R. Sakamoto, A. Tokunaga, Y. Nakatake, M. Sato, and N. Yoshida. 2009. Polypyrimidine tract-binding protein is essential for early mouse development and embryonic stem cell proliferation. *The FEBS Journal*. 276:6658–6668. doi:10.1111/j.1742-4658.2009.07380.x.

Shinkai, Y., G. Rathbun, K.P. Lam, E.M. Oltz, V. Stewart, M. Mendelsohn, J. Charron, M. Datta, F. Young, and A.M. Stall. 1992. RAG-2-deficient mice lack mature lymphocytes owing to inability to initiate V(D)J rearrangement. *Cell*. 68:855–867.

Spellman, R., M. Llorian, and C.W.J. Smith. 2007. Crossregulation and functional redundancy between the splicing regulator PTB and its paralogs nPTB and ROD1. *Molecular Cell*. 27:420–434. doi:10.1016/j.molcel.2007.06.016.

Suckale, J., O. Wendling, J. Masjkur, M. Jäger, C. Münster, K. Anastassiadis, A.F. Stewart, and M. Solimena. 2011. PTBP1 is required for embryonic development before gastrulation. *PLoS ONE*. 6:e16992. doi:10.1371/journal.pone.0016992.

Susaki, E., K. Nakayama, and K.I. Nakayama. 2007. Cyclin D2 Translocates p27 out of the Nucleus and Promotes Its Degradation at the G0-G1 Transition. *Mol. Cell. Biol.* 27:4626–4640. doi:10.1128/MCB.00862-06.

Thompson, B.J., R. Bhansali, L. Diebold, D.E. Cook, L. Stolzenburg, A.-S. Casagrande, T. Besson, B. Leblond, L. Désiré, S. Malinge, and J.D. Crispino. 2015. DYRK1A controls the transition from proliferation to quiescence during lymphoid development by destabilizing Cyclin D3. *Journal of Experimental Medicine*. 212:953–970. doi:10.1084/jem.20150002.

Trapnell, C., A. Roberts, L. Goff, G. Pertea, D. Kim, D.R. Kelley, H. Pimentel, S.L. Salzberg, J.L. Rinn, and L. Pachter. 2012. Differential gene and transcript expression analysis of RNA-seq experiments with TopHat and Cufflinks. *Nat Protoc*. 7:562–578. doi:10.1038/nprot.2012.016.

Vuong, J.K., C.-H. Lin, M. Zhang, L. Chen, D.L. Black, and S. Zheng. 2016. PTBP1 and PTBP2 Serve Both Specific and Redundant Functions in Neuronal Pre-mRNA Splicing. *Cell Reports*. 17:2766–2775. doi:10.1016/j.celrep.2016.11.034.

Yang, W., J. Shen, M. Wu, M. Arsura, M. FitzGerald, Z. Suldan, D.W. Kim, C.S. Hofmann, S. Pianetti, R. Romieu-Mourez, L.P. Freedman, and G.E. Sonenshein. 2001. Repression of transcription of the p27 Kip1 cyclin-dependent kinase inhibitor gene by c-Myc. *Oncogene*. 20:1688–1702. doi:10.1038/sj.onc.1204245.

Yoon, M.-K., D.M. Mitrea, L. Ou, and R.W. Kriwacki. 2012. Cell cycle regulation by the intrinsically disordered proteins p21 and p27. *Biochemical Society Transactions*. 40:981–988. doi:10.1042/BST20120092.

Yüce, Ö., A. Piekny, and M. Glotzer. 2005. An ECT2–centralspindlin complex regulates the localization and function of RhoA. *The Journal of Cell Biology*. 170:571–582. doi:10.1083/jcb.200501097.

Zeman, M.K., and K.A. Cimprich. 2013. Causes and consequences of replication stress. *Nature Cell Biology*. 16:2–9. doi:10.1038/ncb2897.

Zhu, A., J.G. Ibrahim, and M.I. Love. 2019. Heavy-tailed prior distributions for sequence count data: removing the noise and preserving large differences. *Bioinformatics*. 35:2084–2092. doi:10.1093/bioinformatics/bty895.

Figure Legends

Figure 1. Lack of PTBP1 and PTBP2 blocks B cell development.

a, Splenocytes pre-gated on live (eFluor780-) cells. Numbers in plots show proportions of B cells from mice of the indicated genotypes. **b**, Numbers of B cells ($B220^{+}CD19^{+}$) identified as shown in **a** per spleen from mice with the indicated genotypes. Data shown is from one representative out of two independent experiments. **c**, Gating strategy based on cell-surface markers for developing B cells from bone marrow cells pre-gated on dump (Gr-1, CD11b, NK1.1, Siglec-F and F4/80)-negative live ($eFluor780^{-}$) cells. Full gating strategy is shown in **Supplementary Fig. 1f**. **d**, Numbers of developing B cells in the bone marrow (2 femurs and 2 tibias per mouse) of mice with the indicated genotypes. **b**, **d**, Bars depict means, each point represents data from an individual mouse and P-values were calculated by one-way ANOVA with Tukey's multiple comparisons test. Summary adjusted p value *<0.05, **<0.01, ***<0.001, ****<0.0001.

c, **d**, Data shown is from one representative out of three independent experiments with 4 to 5 mice per genotype (except for *Rag2*$^{-/-}$ mice from which one or two mice were included) carried out with the same mouse genotypes shown except for the *CD79a*$^{Cre/+}$*Ptbp1*$^{+/+}$*Ptbp2*$^{+/+}$ mice which were only included in the experiment shown here (three *CD79a*$^{Cre/+}$*Ptbp1*$^{+/+}$*Ptbp2*$^{+/+}$ mice).

Figure 2. Cell cycle progression in Pro-B cells.

a, EdU and BrdU sequential labelling experimental set up to distinguish early, late and post S-phase cells. **b**, Flow cytometry data of the different stages of S-phase in pro-B cells ($B220^{+}CD19^{+}IgD^{-}$surfaceIgM^{-}intracellular-Igμ$^{-}CD43^{high}$) identified as shown in **Supplementary Fig. 3a**. Numbers shown are proportions of cells. **c**, Percentages of pro-

B cells in different S-phase stages determined as shown in **a** and **b**. **d**, Number of pro-B cells in bone marrow (2 femurs and 2 tibias per mouse) at different S-phase stages determined as shown in **b**. **e**, Flow cytometry data of pro-B cells identified as shown in **Supplementary Fig. 3a** and excluding BrdU^{+}-only (cells in early S-phase). Numbers shown are proportions of cells in the G2/M gate. **f**, Proportions and numbers (in 2 femurs and 2 tibias per mouse) of pro-B cells in G2/M identified as shown in **e**. In **c**, **d**, **f**, bars depict means, each point represents data from an individual mouse and P-values were calculated by one-way ANOVA with Tukey's multiple comparisons test. Summary adjusted p-value *<0.05, **<0.01, ***<0.001, ****<0.0001. **b-f**, data shown is from one of two independent experiments.

Figure 3. PTBP1 and PTBP2 absence causes changes in mRNA abundance and AS.

a, Differences in mRNA abundance in pairwise comparisons from pro-B cell transcriptomes. Shown are Log2Fold changes calculated with DESeq2 (**Supplementary Table 3**). Red dots are values from genes with significant differences in mRNA abundance (padj value <0.05) with a Log2Fold change > |0.5|. Grey dots are values from genes with no significant differences (padj >0.05) or with a Log2Fold change < |0.5|. Numbers in plots are the number of genes with increased or decreased mRNA abundance. **b**, Differences in AS in pairwise comparisons from pro-B cells. Shown are inclusion level differences >|0.1| with an FDR<0.05 for different types of alternatively spliced events: skipped exons (SE), mutually exclusive exons (MXE), alternative 5' and 3' splice sites (A5SS and A3SS, respectively), and retained introns (RI), (**Supplementary table 4**) analysed with rMATS. Each dot shows the inclusion level difference for one event. **c**, overlaps of genes that have changes in abundance and AS amongst the indicated pairwise comparisons. **d**, Heatmap shows z-scores of normalised read counts from DESeq2 from

each biological replicate for genes that were found with differential mRNA abundance in any of the three pair-wise comparisons shown in **a**. **e**, Heatmap shows z-scores of inclusion levels from each biological replicate for those AS events that are alternatively spliced in any of the three pair-wise comparisons shown in **b**. **d**, **e**, Hierarchical clustering was done on Euclidean distances from z-scores and is shown with dendrograms.

Figure 4. Lack of global enrichment of proliferation-related terms amongst changes in the transcriptome due to PTBP1 and PTBP2 absence.

a, Selected gene ontology (GO) terms (process and function) significantly (p-value <0.05) enriched amongst genes that are differentially expressed at the abundance or the AS level when comparing the transcriptome of P1P2dKO pro-B cells to P1sKO and control pro-B cells as shown in **Fig. 3d** and **e**. Numbers show how many genes a GO term has. **Supplementary table 5** contains all significantly enriched GO process and function terms. **b**, Log2-fold changes in mRNA abundance in the indicated pair-wise comparisons for all tested genes (all genes), genes with increased abundance in S-phase (S) and G2/M-phases (G2/M). Grey dots show genes with padj>0.05. Red dots amongst "all genes" show genes with padj<0.05 and a >|0.5| log2-fold change. Red dots amongst S and G2M groups show genes with a padj<0.05 regardless of their log2-fold change.

Figure 5. CDK inhibitors and CDK activity in P1P2dKO pro-B cells.

a, mRNA abundance of CDK inhibitors in pro-B cells from control, P1sKO and P1P2dKO mice. Points show DESeq2 normalised read counts from individual pro-B cell mRNAseq libraries. Bars depict means. DESeq2 calculated p-adjusted values are shown when <0.05 for the indicated pairwise comparisons. **b**, Intracellular flow cytometry with anti-p27 antibody or control isotype staining detected with an anti-rabbit AF647 conjugated

secondary antibody. **c**, Median fluorescence intensities (MFI) from staining shown in **b**. **d**, Intracellular flow cytometry with the indicated antibodies. Numbers show proportions of gated events. **e**, Proportions of cells identified as in **d**. **b**, **d**, Each histogram line shows data from an individual mouse with the indicated genotype. FrB pro-B cells in G0/G1, S or G2/M phases of the cell cycle were defined by EdU incorporation and DNA staining as shown in **Supplementary Fig. 3g. c**, **e**, Points show data from individual mice. Bars depict the mean. P-values were calculated by two-way ANOVA with Tukey's multiple comparisons test. Summary adjusted p value *<0.05, **<0.01, ***<0.001, ****<0.0001.

b – e, Data is from one experiment with four to five mice per genotype. The differences observed for pT592-SAMHD1 and pS807/S811-RB between control and P1P2dKO cells were confirmed in an independent experiment where two control and two P1P2dKO mice were used.

Figure 6. Cell cycle regulators in the absence of PTBP1 and PTBP2.

a, mRNA abundance of cell cycle regulators in pro-B cells from control, P1sKO and P1P2dKO mice. Genes whose names are in yellow and bold are predicted to have reduced mRNA abundance due to changes in AS upon *Ptbp1* and *Ptbp2* deletion. Individual data points show DESeq2 normalised read counts from individual pro-B cell mRNAseq libraries. Bars depict means. DESeq2 calculated adjusted p-values are shown when <0.05 for the indicated pairwise comparisons. **b**, PTBP1 iCLIP and mRNAseq data visualisation. For PTBP1 iCLIP, x-link sites are shown for all events. Clusters of PTBP1 binding are shown when found. mRNAseq data from pro-B cells of one replicate per genotype is shown using sashimi plot visualisation from IGV. Numbers on the left show the maximum number of reads in the coverage plots. Arcs depict exon-exon junctions detected in mRNAseq reads. Numbers in arcs show the number of reads for the depicted exon-exon

junction. Parts of transcript isoforms predicted to be degraded by NMD are shown in yellow. Parts of transcript isoforms coding for proteins are shown in blue. Exon numbers of transcript isoforms coding for proteins are shown with E and a number. **c**, mRNAseq visualisation as in **b** from HeLa control cells or cells where PTBP1 and PTBP2 were knocked down (Ling et al., 2016). **d**, Human *RBL1* normalised DESeq2 read counts from the two mRNAseq libraries (one control and 1 double knock down) shown in **c**. **e**, Representation of cell cycle mRNA regulon controlled by PTBP1 in pro-B cells and consequences of *Ptbp1* and *Ptbp2* deletion in pro-B cells. Depicted interactions of PTBP1 with individual factors are likely to be direct.

SUPPLEMENTARY FIGURES:

Supplementary Figure 1. PTBPs expression in developing B cells.

a, Representation of B cell development in the bone marrow using the Philadelphia nomenclature (Hardy and Hayakawa, 2003) including Hardy's fractions (Fr) based on cell-surface markers (Hardy et al., 1991). **b**, Identification strategy of bone marrow cells using cell-surface and intracellular markers. **c**, PTBP1, PTBP2 and PTBP3 expression analysed by flow cytometry. Identification of different B cell developmental stages was carried out as shown in **b**. **d**, Geometric fluorescence mean intensity (gMFI) of staining for PTBP1, PTBP1, PTBP3 and control isotypes as shown in **c**. Bars depict means. Each data point shows data from an individual control mouse (*CD79a*$^{+/+}$*Ptbp1*$^{fl/fl}$*Ptbp2*$^{fl/fl}$). Data shown is from one experiment with 5 mice. **e**, Numbers and proportions of B cells (eFluor780^{-}B220^{+}CD19^{+}) in mesenteric lymph nodes. **f**, Complete gating strategy of cells from bone marrow using cell surface markers to identify developing B cells and Hardy's fractions B, C and C' as shown in **Fig. 1c**. Dump contains Gr-1, CD11b, NK1.1, Siglec-F and

F4/80. Data shown is from a Ctrl (*CD79a*$^{+/+}$*Ptbp1*$^{fl/fl}$*Ptbp2*$^{fl/fl}$) mouse. **b**, **f**, numbers indicate proportions of gated populations.

Supplementary Figure 2. B cell development characterisation in the absence of PTBP1 and PTBP2

a, Cell surface and intracellular staining strategy to define B cell developmental stages in bone marrow cells from mice of the indicated genotypes. Numbers shown are percentages of gated events. **b**, PTBP1, PTBP2 and PTBP3 detection and negative isotype control staining in different B cell developmental stages identified as shown in **a**. Data shown is of a representative mouse out of five for each genotype indicated. Data shown is from one experiment. **c**, c-KIT and CD2 expression at different B cell developmental stages in mice of the indicated genotypes. Identification of different B cell developmental stages was done as shown in **Supplementary Fig. 1f**. **a, b, c,** data shown is representative from one mouse out of five mice per genotype, except for *Rag2*$^{-/-}$ mice for which only two were included. **d**, c-KIT median fluorescence intensity (MFI) in pro-B cells (FrB and FrC) identified as shown in **c**. **c, d**, Data shown is from one out of three independent experiments. **e**, Numbers of developing B cells in bone marrow from two femurs and two tibias identified as shown in **a** with a combination of cell-surface and intracellular staining. Data shown is from one experiment. **d, e** Bars show means, each point represents data from an individual mouse, P-values were calculated by one-way ANOVA with Tukey's multiple comparisons test. Summary adjusted p value *<0.05, **<0.01, ***<0.001, ****<0.0001.

Supplementary Figure 3. Cell cycle analysis in developing B cells.

a, Gating strategy identifying pre-pro-, pro- and early-pre-B cells in EdU and BrdU sequential labelling experiments for bone marrow live cells from the indicated genotypes. **b**, Early-, late- and post-S-phase gating amongst pre-pro-, pro- and early-pre-B cells identified as shown in **a**. **c**, Proportions of early, late and post S-phase cells amongst pre-pro-, pro- and early-pre-B cells identified as shown in **a** and **b**. **d**, Numbers of early-, late- and post-S-phase pre-pro-, pro- and early-pre-B cells identified as shown in **a** and **b** in two tibias and two femurs per mouse. **e**, Gating strategy to identify cells in G2/M phases amongst pre-pro-, pro- and early-pre-B cells identified as shown in **a**. Events shown are pre-gated excluding cells in early S-phase ($BrdU^+$-only). **f**, Proportions and numbers (in two tibias and two femurs per mouse) of G2/M pre-pro-, pro- and early-pre-B cells identified as shown in **a** and **e**. **g**, Identification strategy of proliferating FrB pro-B cells amongst bone marrow cells from mice with the indicated genotypes. Mice were injected with EdU i.p. for one hour before analysis to track cells in G0/G1, S and G2/M phases of the cell cycle. **h**, Proportions of FrB developing B cells in G0/G1, S and G2/M phases defined as shown in **g**. **i**, Phospho-histone 3 serine 10 (pH3 S10) staining amongst FrB pro-B cells identified as in **g**. **j**, Percentages of pH3(S10)-positive cells amongst cells with duplicated DNA amounts (4n) in pro-B cells (FrB) assessed by flow cytometry as shown in **i**. **a**, **b**, **e**, **g**, **i**, Numbers shown indicate proportions. **c**, **d**, **f**, **h**, **j** Bars show means, each point shows data from an individual mouse and P-values were calculated by one-way ANOVA with Tukey's multiple comparisons test. Summary adjusted p value *<0.05, **<0.01, ***<0.001, ****<0.0001. **c**, **d**, **f**, Data shown is from one out of two independent experiments. **h**, **j**, Data shown is from one out of three independent similar experiments.

Supplementary Figure 4. DNA-damage assessment in PTBP1 and PTBP2 deficient FrB pro-B cells.

a, FCS-A measurements of FrB pro-B cells in different phases of the cell cycle identified as in **Supplementary Fig. 3g**. **b**, Intracellular staining with anti-pH2AX or an isotype control. **c**, MFIs (median fluorescence intensity) from the staining shown in **b** and fold changes in MFIs from intracellular staining with pH2AX and isotype control antibodies between FrB pro-B cells from P1sKO (*CD79a*$^{Cre/+}$*Ptbp1*$^{fl/fl}$*Ptbp2*$^{+/+}$) and control (Ctrl, *CD79a*$^{+/+}$*Ptbp1*$^{fl/fl}$*Ptbp2*$^{fl/fl\ or\ +/+}$) mice or from P1P2dKO (*CD79a*$^{Cre/+}$*Ptbp1*$^{fl/fl}$*Ptbp2*$^{fl/fl}$) and control mice in different cell cycle phases from the data shown in **b**. **d,** Intracellular staining with anti-pH2AX FrB pro-B cells in different cell cycle phases. Bone marrow cells were either stained on their cell surface to identify FrB pro-B cells and fixed before intracellular staining, EdU and DNA detection (ex vivo) or were incubated with 20 μM Etoposide in RPMI at 37°C for 3 hours before cell surface staining to identify FrB pro-B cells (+Etoposide). **f**, MFIs from staining shown in **d** and fold changes in MFIs calculated as described in **c**. **f**, Intracellular staining with anti-p53 antibody or with an isotype control in FrB pro-B cells. Cells were analysed after isolation from the bone marrow (ex vivo) or after treatment with etoposide as described in **d**. **g**, MFIs from the staining shown in **f** and fold change in MFI for the different staining as described in **c**. In **a**, **b**, **d**, and **f** FrB pro-B cells were identified in different phases of the cell cycle by EdU incorporation and DNA staining as shown in **Supplementary Fig. 3g**. In **a**, **b**, **d** and **f**, each histogram line shows data from an individual mouse. In **a**, **c**, **e** and **g** Each point shows data from an individual mouse. Bars show means. P-values were calculated by two-way ANOVA with Tukey's multiple comparisons test. Summary adjusted p value *<0.05, **<0.01, ***<0.001, ****<0.0001. **a**, data shown is representative from one out of three independent experiments. **b**, **c**, Data is representative from one out of two independent experiments. **d, e, f, g** data shown is from one experiment where the treatment with etoposide was included. Differences in p53 staining levels between FrB pro-B cells from P1P2dKO and

control mice were confirmed in an independent experiment where two P1P2dKO mice and two control mice were analysed.

Supplementary Figure 5. Cell sorting strategy of pro-B cells.

a, Cell sorting strategy of FrB pro-B ($B220^{+}CD19^{+}IgM^{-}IgD^{-}CD2^{-}CD43^{high}CD25^{-}cKIT^{+}CD24^{+}CD249^{+}$) cells used to isolate RNA and carry out mRNAseq libraries. Dump contains IgM, CD2 and streptavidin. Prior sorting, bone marrow cells were depleted from Gr-1, CD11b, IgD, NK1.1, CD3e and Ter119-positive cells.

Supplementary Figure 6. Transcriptome analysis of pro-B cells.

a, Transcriptome correlation in mitogen-activated primary B cells and FrB pro-B cells. Dots show mean values of TPMs (transcripts per million) from four or five biological replicates in mitogen-activated B cells and pro-B cells, respectively. Correlation was calculated with Spearman's rank correlation rho on genes with >= 1 TPM in pro-B cells and >0 TPM in mitogen-activated B cells (12545 genes). 681 genes had 0 TPMs in mitogen-activated B cells and >=1 TPM in pro-B cells. **b**, Proportions of genes with differences in mRNA abundance for the indicated pairwise comparisons that are bound by clusters of PTBP1 (iCLIP data) on their 3'UTR (**Supplementary Tables 2** and **3**). **c**, *Ptbp2* mRNAseq visualisation with Sashimi coverage plots done with IGV showing one replicate per genotype. Arches depict reads mapping to two different exons. Numbers on arches show the number of reads that map to that particular exon-exon junction. Numbers in black on the left show the maximum number of reads in the coverage plots.

d, Different types of alternatively spliced events analysed with rMATS. **e**, Proportions of AS changes between the indicated comparisons that are bound by at least one PTBP1 cluster in the vicinity of the alternatively spliced event (see methods for definition of

vicinity, **Supplementary Tables 2** and **4**). **f**, mRNA abundance of B cell development regulators in pro-B cells. DESeq2 normalised read counts of the indicated genes. DESeq2 calculated padj values are shown when <0.05. Bars show means. Each dot shows data from an individual mRNAseq biological replicate.

Supplementary Figure 7. PTBP1 binding to target transcripts

a, PTBP1 binding (iCLIP data) to 3'UTRs. **b**, Intracellular c-MYC or control isotype staining of FrB pro-B cells in different stages of the cell cycle identified as shown in **Supplementary Fig. 3g**. Each line shows data from one individual mouse. **c**, Median fluorescence intensities (MFI) from the staining shown in **b**. Each point shows data from an individual mouse. Bars show means. P-values were calculated by two-way ANOVA with Tukey's multiple comparisons test. Summary adjusted p value *<0.05, **<0.01, ***<0.001, ****<0.0001. Data shown is from one representative out of two independent experiments.

SUPPLEMENTARY TABLES:

Supplementary Table 1. PTBP1 binding sites (xlinks).

Supplementary Table 2. PTBP1 binding sites (clusters).

Supplementary Table 3. mRNA abundance analysis. DESeq2 results shown in Fig. 3a. Separate tabs show genes with significant differential (padj<0.05) mRNA abundance with a log2 fold change > |0.5| for the different pairwise comparisons carried out and also all the results obtained with DESeq2. Additional tabs shown genes whose transcripts were bound by PTBP1 clusters at their 3'UTR.

Supplementary Table 4. AS analysis. Different tabs show inclusion level differences (IncLevelDifference) shown in Fig. 3b for the three pairwise comparisons carried out. The first three tabs show significant (FDR <0.05) alternatively spliced events with an absolute inclusion level difference >0.1. "allresults" tabs show all the results from rMATS. "PTBP1 bound" tabs show those significantly differentially spliced events that were bound in their vicinity by PTBP1 clusters.

Supplementary table 5. Gene ontology enrichment analysis. Results from gene ontology enrichment analysis carried out with the groups of genes identified in **Fig. 3d, e**.

Supplementary Table 6. DESeq2 results for genes shown to have high mRNA expression levels in S or G2M phases (Giotti et al., 2018) in the three pair-wise comparisons shown in **Fig. 4b**.

Supplementary Table 7. Antibodies and reagents used in flow cytometry experiments.

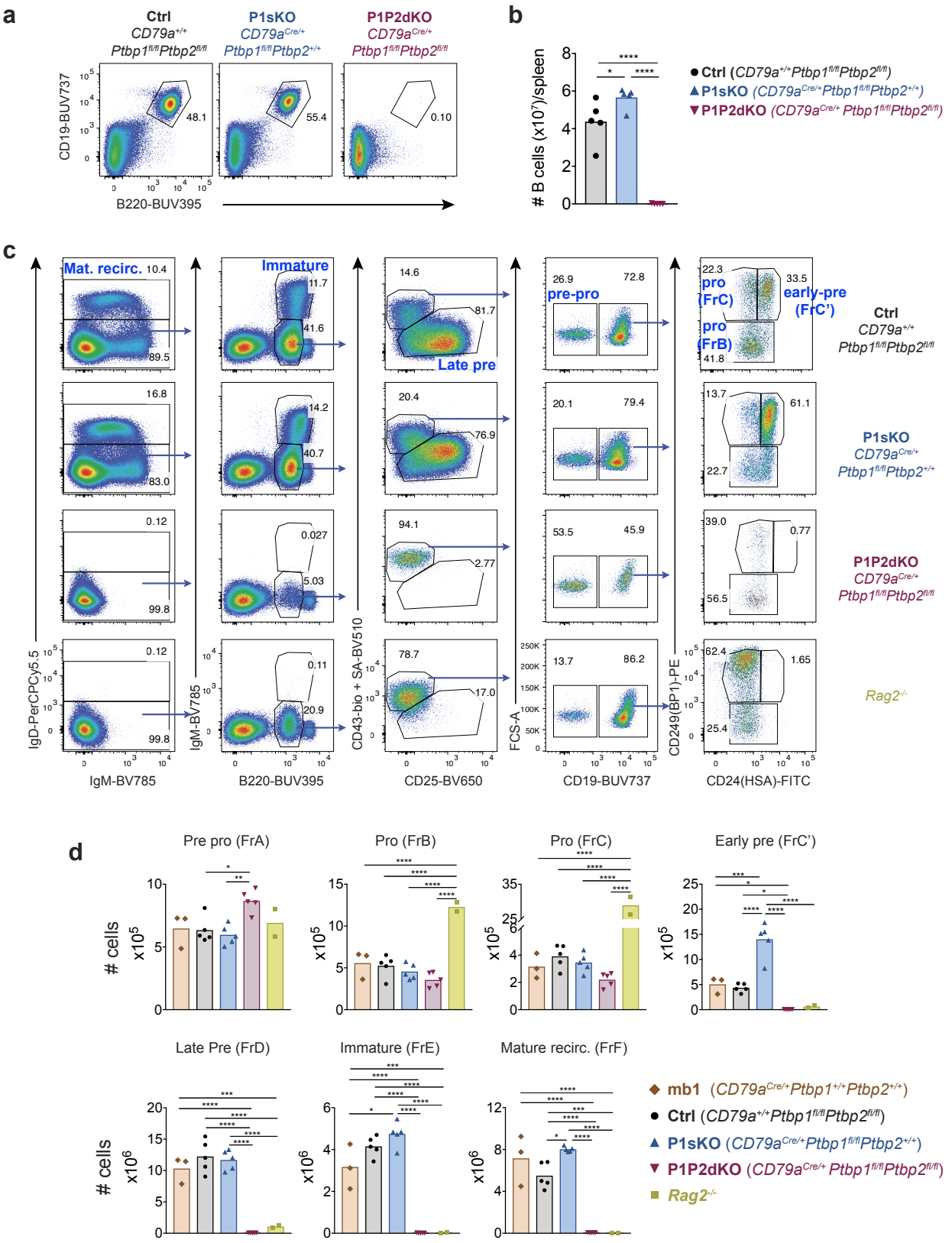
a
Ctrl
CD79a+/+
Ptbp1fl/flPtbp2fl/fl
P1sKO
CD79aCre/+
Ptbp1fl/flPtbp2+/+
P1P2dKO
CD79aCre/+
Ptbp1fl/flPtbp2fl/fl
CD19-BUV737
B220-BUV395
48.1
55.4
0.10
b
B cells (x10^7)/spleen
Ctrl (CD79a+/+Ptbp1fl/flPtbp2fl/fl)
P1sKO (CD79aCre/+Ptbp1fl/flPtbp2+/+)
P1P2dKO (CD79aCre/+ Ptbp1fl/flPtbp2fl/fl)
c
Mat. recirc.
Immature
Late pre
pre-pro
pro (FrC)
pro (FrB)
early-pre (FrC')
Ctrl
P1sKO
P1P2dKO
Rag2-/-
IgD-PerCPCy5.5
IgM-BV785
B220-BUV395
CD43-bio + SA-BV510
CD25-BV650
FCS-A
CD19-BUV737
CD249(BP1)-PE
CD24(HSA)-FITC
d
Pre pro (FrA)
Pro (FrB)
Pro (FrC)
Early pre (FrC')
Late Pre (FrD)
Immature (FrE)
Mature recirc. (FrF)
cells
mb1 (CD79aCre/+Ptbp1+/+Ptbp2+/+)
Ctrl (CD79a+/+Ptbp1fl/flPtbp2fl/fl)
P1sKO (CD79aCre/+Ptbp1fl/flPtbp2+/+)
P1P2dKO (CD79aCre/+ Ptbp1fl/flPtbp2fl/fl)
Rag2-/-

Figure 1

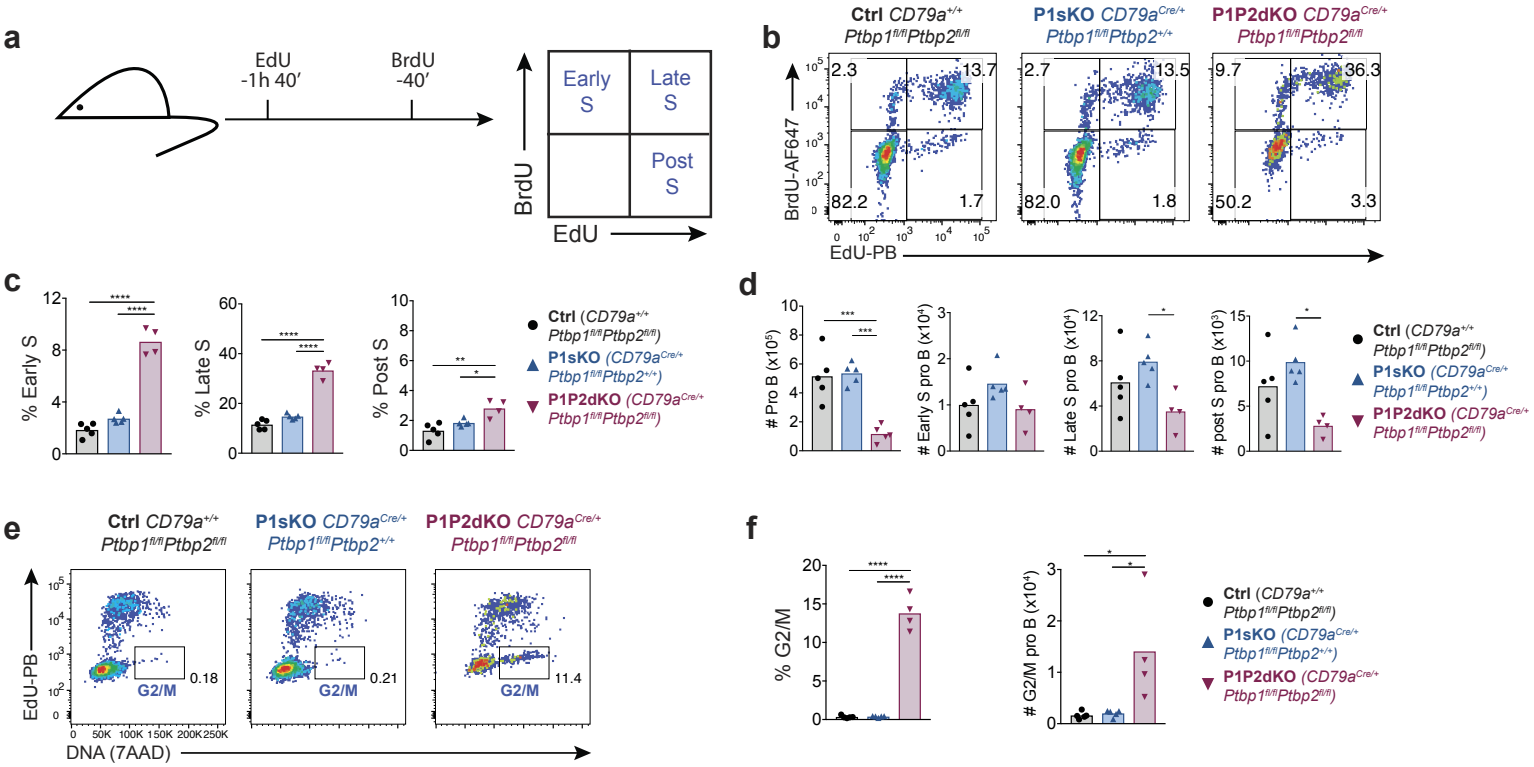
a
EdU
-1h 40′
BrdU
-40′
Early S
Late S
Post S
BrdU
EdU
b
Ctrl CD79a+/+ Ptbp1fl/flPtbp2fl/fl
P1sKO CD79aCre/+ Ptbp1fl/flPtbp2+/+
P1P2dKO CD79aCre/+ Ptbp1fl/flPtbp2fl/fl
BrdU-AF647
EdU-PB
2.3
13.7
82.2
1.7
2.7
13.5
82.0
1.8
9.7
36.3
50.2
3.3
c
% Early S
% Late S
% Post S
Ctrl (CD79a+/+ Ptbp1fl/flPtbp2fl/fl)
P1sKO (CD79aCre/+ Ptbp1fl/flPtbp2+/+)
P1P2dKO (CD79aCre/+ Ptbp1fl/flPtbp2fl/fl)
d
Pro B (x10⁵)
Early S pro B (x10⁴)
Late S pro B (x10⁴)
post S pro B (x10⁴)
e
Ctrl CD79a+/+ Ptbp1fl/flPtbp2fl/fl
P1sKO CD79aCre/+ Ptbp1fl/flPtbp2+/+
P1P2dKO CD79aCre/+ Ptbp1fl/flPtbp2fl/fl
EdU-PB
DNA (7AAD)
G2/M
0.18
0.21
11.4
f
% G2/M
# G2/M pro B (x10⁴)
Ctrl (CD79a+/+ Ptbp1fl/flPtbp2fl/fl)
P1sKO (CD79aCre/+ Ptbp1fl/flPtbp2+/+)
P1P2dKO (CD79aCre/+ Ptbp1fl/flPtbp2fl/fl)

Figure 2

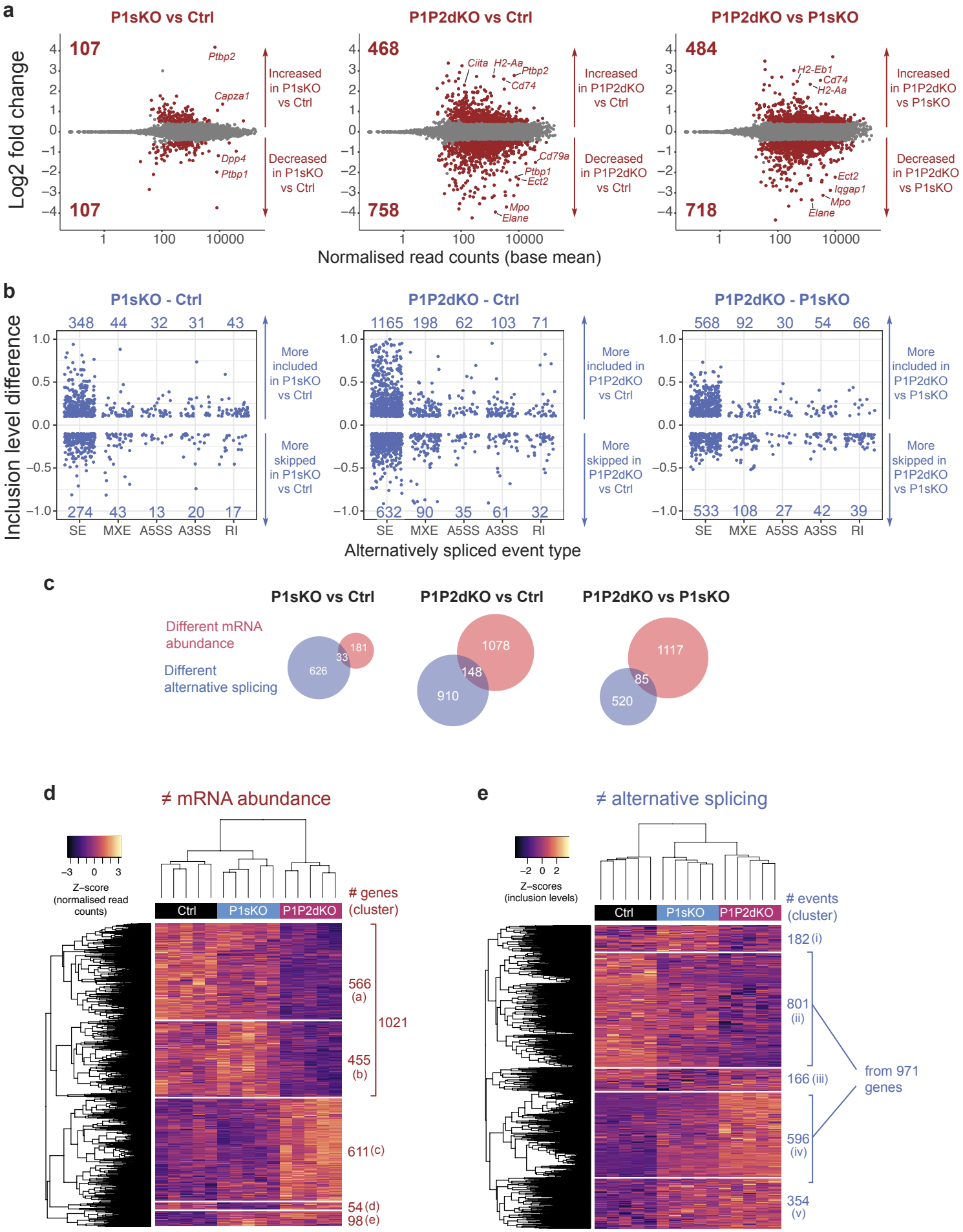
a
P1sKO vs Ctrl
P1P2dKO vs Ctrl
P1P2dKO vs P1sKO
Log2 fold change
107
107
468
758
484
718
Ptbp2
Capza1
Dpp4
Ptbp1
Ciita
H2-Aa
Ptbp2
Cd74
Cd79a
Ptbp1
Ect2
Mpo
Elane
H2-Eb1
Cd74
H2-Aa
Ect2
Iqgap1
Mpo
Elane
Increased in P1sKO vs Ctrl
Decreased in P1sKO vs Ctrl
Increased in P1P2dKO vs Ctrl
Decreased in P1P2dKO vs Ctrl
Increased in P1P2dKO vs P1sKO
Decreased in P1P2dKO vs P1sKO
Normalised read counts (base mean)
b
P1sKO - Ctrl
P1P2dKO - Ctrl
P1P2dKO - P1sKO
Inclusion level difference
348 44 32 31 43
274 43 13 20 17
1165 198 62 103 71
632 90 35 61 32
568 92 30 54 66
533 108 27 42 39
SE MXE A5SS A3SS RI
More included in P1sKO vs Ctrl
More skipped in P1sKO vs Ctrl
More included in P1P2dKO vs Ctrl
More skipped in P1P2dKO vs Ctrl
More included in P1P2dKO vs P1sKO
More skipped in P1P2dKO vs P1sKO
Alternatively spliced event type
c
P1sKO vs Ctrl
P1P2dKO vs Ctrl
P1P2dKO vs P1sKO
Different mRNA abundance
Different alternative splicing
181
33
626
1078
148
910
1117
85
520
d
≠ mRNA abundance
Z–score (normalised read counts)
Ctrl
P1sKO
P1P2dKO
genes (cluster)
566 (a)
455 (b)
1021
611 (c)
54 (d)
98 (e)
e
≠ alternative splicing
Z–scores (inclusion levels)
events (cluster)
182 (i)
801 (ii)
166 (iii)
596 (iv)
354 (v)
from 971 genes

Figure 3

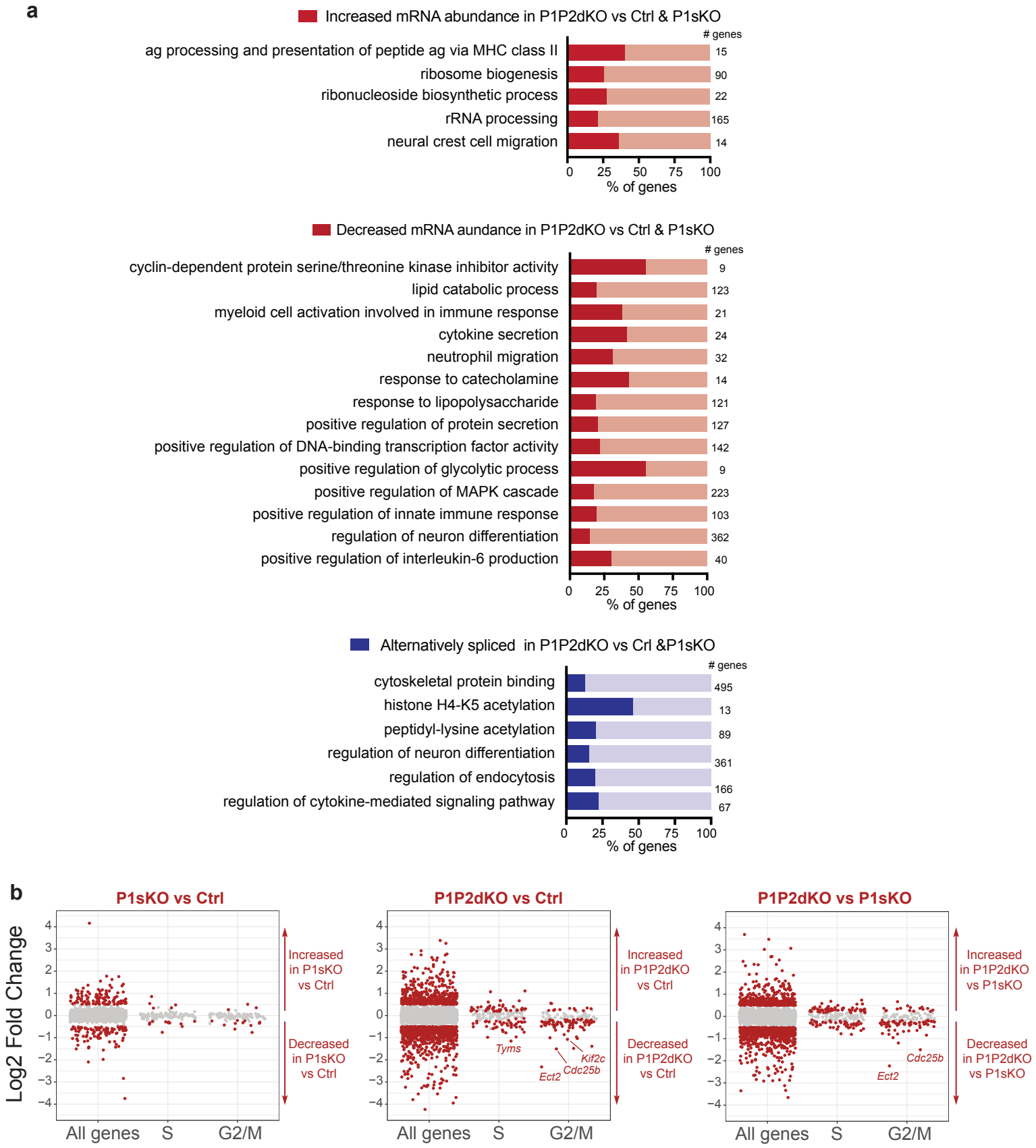
a
Increased mRNA abundance in P1P2dKO vs Ctrl & P1sKO
genes
ag processing and presentation of peptide ag via MHC class II
ribosome biogenesis
ribonucleoside biosynthetic process
rRNA processing
neural crest cell migration
15
90
22
165
14
0 25 50 75 100
% of genes
Decreased mRNA aundance in P1P2dKO vs Ctrl & P1sKO
genes
cyclin-dependent protein serine/threonine kinase inhibitor activity
lipid catabolic process
myeloid cell activation involved in immune response
cytokine secretion
neutrophil migration
response to catecholamine
response to lipopolysaccharide
positive regulation of protein secretion
positive regulation of DNA-binding transcription factor activity
positive regulation of glycolytic process
positive regulation of MAPK cascade
positive regulation of innate immune response
regulation of neuron differentiation
positive regulation of interleukin-6 production
9
123
21
24
32
14
121
127
142
9
223
103
362
40
0 25 50 75 100
% of genes
Alternatively spliced in P1P2dKO vs Crl &P1sKO
genes
cytoskeletal protein binding
histone H4-K5 acetylation
peptidyl-lysine acetylation
regulation of neuron differentiation
regulation of endocytosis
regulation of cytokine-mediated signaling pathway
495
13
89
361
166
67
0 25 50 75 100
% of genes
b
P1sKO vs Ctrl
P1P2dKO vs Ctrl
P1P2dKO vs P1sKO
Log2 Fold Change
Increased in P1sKO vs Ctrl
Decreased in P1sKO vs Ctrl
Increased in P1P2dKO vs Ctrl
Decreased in P1P2dKO vs Ctrl
Increased in P1P2dKO vs P1sKO
Decreased in P1P2dKO vs P1sKO
Tyms
Kif2c
Ect2
Cdc25b
All genes
S
G2/M

Figure 4

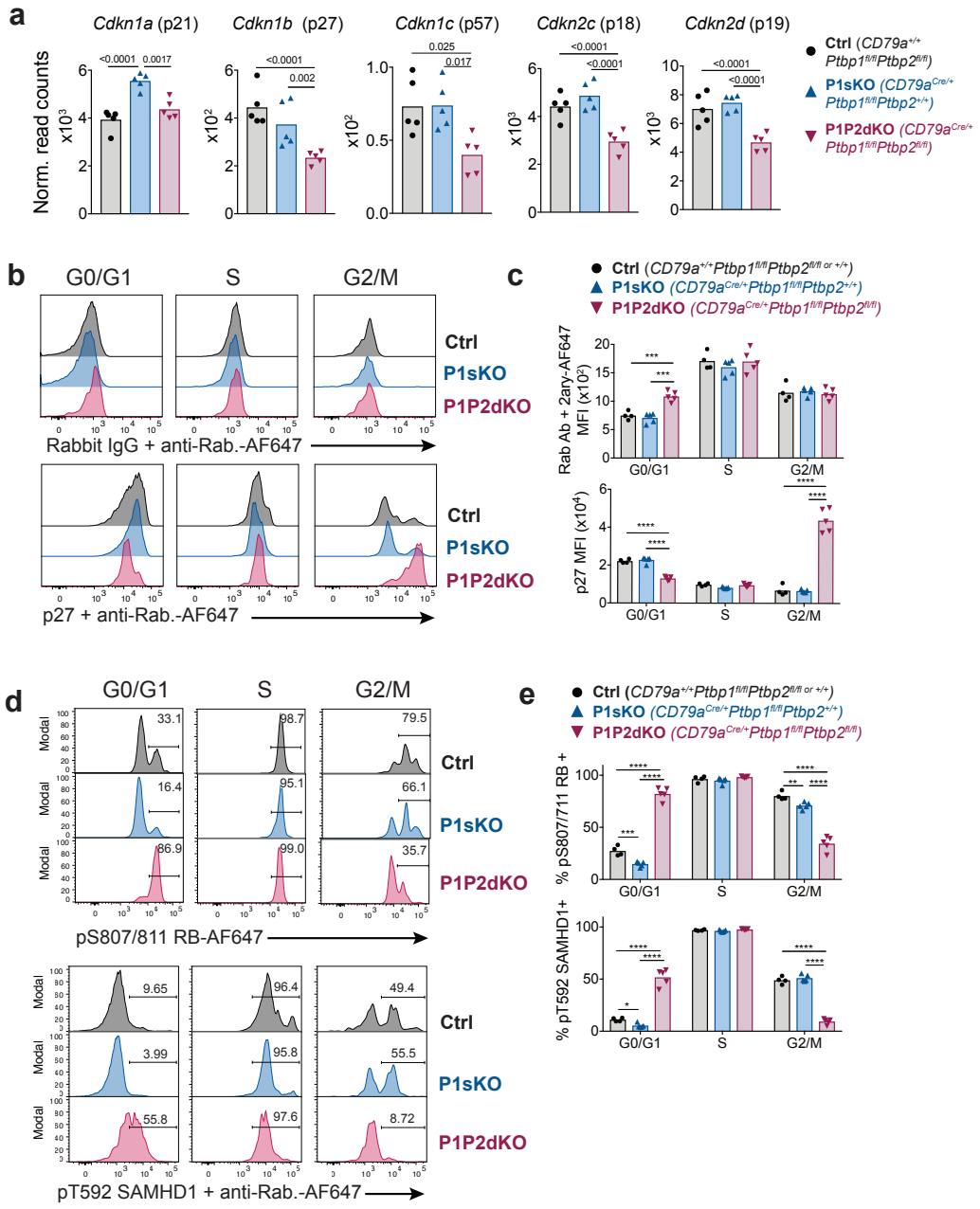
a
Cdkn1a (p21)
Cdkn1b (p27)
Cdkn1c (p57)
Cdkn2c (p18)
Cdkn2d (p19)
Norm. read counts
Ctrl (CD79a+/+ Ptbp1fl/flPtbp2fl/fl)
P1sKO (CD79aCre/+ Ptbp1fl/flPtbp2+/+)
P1P2dKO (CD79aCre/+ Ptbp1fl/flPtbp2fl/fl)
b
G0/G1
S
G2/M
Ctrl
P1sKO
P1P2dKO
Rabbit IgG + anti-Rab.-AF647
p27 + anti-Rab.-AF647
c
Rab Ab + 2ary-AF647 MFI (x10²)
p27 MFI (x10⁴)
d
pS807/811 RB-AF647
pT592 SAMHD1 + anti-Rab.-AF647
e
% pS807/711 RB +
% pT592 SAMHD1+

Figure 5

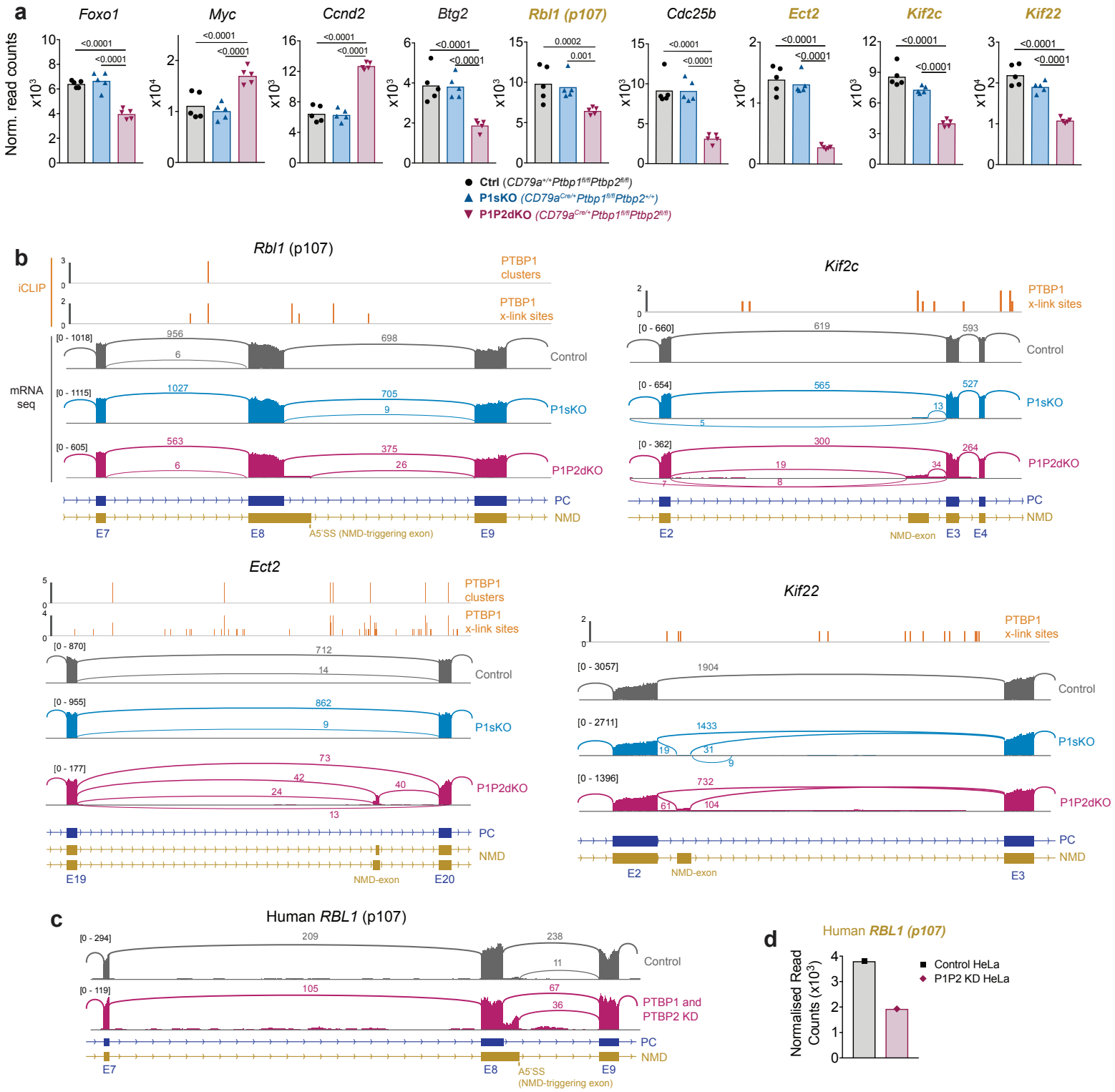
a
Foxo1
Myc
Ccnd2
Btg2
Rbl1 (p107)
Cdc25b
Ect2
Kif2c
Kif22
Norm. read counts
<0.0001
0.0002
0.001
Ctrl (CD79a+/+Ptbp1fl/flPtbp2fl/fl)
P1sKO (CD79aCre/+Ptbp1fl/flPtbp2+/+)
P1P2dKO (CD79aCre/+Ptbp1fl/flPtbp2fl/fl)
b
Rbl1 (p107)
iCLIP
PTBP1 clusters
PTBP1 x-link sites
mRNA seq
Control
P1sKO
P1P2dKO
PC
NMD
E7
E8
A5'SS (NMD-triggering exon)
E9
Kif2c
E2
NMD-exon
E3
E4
Ect2
E19
E20
Kif22
c
Human RBL1 (p107)
PTBP1 and PTBP2 KD
A5'SS (NMD-triggering exon)
d
Human RBL1 (p107)
Normalised Read Counts (x10³)
Control HeLa
P1P2 KD HeLa
e
pro B cells - little proliferation
PTBP1 & PTBP2 deficient pro B cells enhanced entry into S & block at G2
FOXO1
c-MYC
CYCLIN D2
CDK 4,6
p27
p107
RB
E2F
Ccna2, Ccne1... Cdk1, Cdk2
KIF2c
KIF22
ECT2
G0
G1
S
G2
M
CYCLIN A,E
CDK 2
TYMS
CYCLIN A,B
CDK 1
CDC25B
SMADH1
pT592

Figure 6